2016

A Lithium Battery Current Estimation Technique Using an Unknown Input Observer

Daniel Cambron
University of Kentucky, danielcambron11@gmail.com
Digital Object Identifier: http://dx.doi.org/10.13023/ETD.2016.062

STUDENT AGREEMENT:

I represent that my thesis or dissertation and abstract are my original work. Proper attribution has been given to all outside sources. I understand that I am solely responsible for obtaining any needed copyright permissions. I have obtained needed written permission statement(s) from the owner(s) of each third-party copyrighted matter to be included in my work, allowing electronic distribution (if such use is not permitted by the fair use doctrine) which will be submitted to UKnowledge as Additional File.

I hereby grant to The University of Kentucky and its agents the irrevocable, non-exclusive, and royalty-free license to archive and make accessible my work in whole or in part in all forms of media, now or hereafter known. I agree that the document mentioned above may be made available immediately for worldwide access unless an embargo applies.

I retain all other ownership rights to the copyright of my work. I also retain the right to use in future works (such as articles or books) all or part of my work. I understand that I am free to register the copyright to my work.

REVIEW, APPROVAL AND ACCEPTANCE

The document mentioned above has been reviewed and accepted by the student's advisor, on behalf of the advisory committee, and by the Director of Graduate Studies (DGS), on behalf of the program; we verify that this is the final, approved version of the student's thesis including all changes required by the advisory committee. The undersigned agree to abide by the statements above.

Daniel Cambron, Student

Dr. Aaron Cramer, Major Professor

Dr. Caicheng Lu, Director of Graduate Studies

A LITHIUM BATTERY CURRENT ESTIMATION TECHNIQUE USING AN UNKNOWN INPUT OBSERVER

THESIS

A thesis submitted in partial fulfillment
of the requirements for the degree of
Master of Science in Electrical
Engineering in the College of
Engineering at the University of
Kentucky

By

Daniel Clay Cambron

Lexington, Kentucky

Director: Dr. Aaron Cramer

Lexington, Kentucky

2016

ABSTRACT OF THESIS

A LITHIUM BATTERY CURRENT ESTIMATION TECHNIQUE USING AN UNKNOWN INPUT OBSERVER

Current consumption measurements are useful in a wide variety of applications, including power monitoring and fault detection within a lithium battery management system (BMS). This measurement is typically taken using either a shunt resistor or a Hall-effect current transducer. Although both methods have achieved accurate current measurements, shunt resistors have inherent power loss and often require isolation circuitry, and Hall-effect sensors are generally expensive. This work explores a novel alternative to sensing battery current by measuring terminal voltages and cell temperatures and using an unknown input observer (UIO) to estimate the battery current. An accurate model of a $LiFePO_4$ cell is created and is then used to characterize a model of the proposed current estimation technique. Finally, the current estimation technique is implemented in hardware and tested in an online BMS environment. Results show that the current estimation technique is sufficiently accurate for a variety of applications including fault detection and power profiling.

KEYWORDS: Current Estimation, Battery Management System, Unknown Input Observer, Lithium Battery, State of Charge

Daniel Cambron

April 20, 2016

A LITHIUM BATTERY CURRENT ESTIMATION TECHNIQUE USING AN UNKNOWN INPUT OBSERVER

By
Daniel Clay Cambron

Aaron Cramer

Director of Thesis

Caicheng Lu

Director of Graduate Studies

April 20, 2016

For Syd

ACKNOWLEDGEMENTS

The following thesis, while an individual work, benefited from the insights and direction of several people. First, my Thesis Chair, Dr. Aaron Cramer, exemplifies the high quality scholarship to which I aspire. He provided timely and instructive comments and evaluation at every stage of the thesis process, allowing me to complete this project on schedule. Next, I wish to thank the complete Thesis Committee: Dr. Aaron Cramer, Dr. Bruce Walcott, and Dr. Yuan Liao. Each individual provided insights that guided and challenged my thinking, substantially improving the finished product.

TABLE OF CONTENTS

LIST OF TABLES

LIST OF FIGURES

CHAPTER ONE: INTRODUCTION

Lithium batteries continue to gain popularity for use in a wide range of markets, from small consumer electronics to full-sized electric vehicles. In every case, a battery management system (BMS) must be employed to protect lithium cells from abuse such as over-charge because an abused cell can exhibit dangerous conditions such as fire, excessive heating, or gaseous discharge. BMSs protect lithium battery packs by taking, at a minimum, terminal voltage and temperature measurements on the cells within a battery pack and limiting the charge and discharge current accordingly in order to prevent dangerous conditions from developing [1]. Increasingly, BMSs also take current measurements that can be used for state of charge calculations, power profiling, as well as fault detection. Current measurements are typically taken using a shunt resistor or a Hall-effect sensor, both of which has their advantages. A shunt resistor is generally inexpensive and can be extremely accurate, but it generally requires additional isolated measurement circuitry for some practical implementations and inherently consumes power due to the series resistance added to the battery system. Hall-effect sensors provide isolated current measurements but are typically less accurate and more expensive [2]. Thus, there remains an opportunity for an effective, yet inexpensive, solution for determining the current consumption of a lithium battery pack.

In this work, a novel technique for determining current consumption is proposed. In essence, the equivalent series resistance (ESR) of a battery cell could be used in place of a dedicated shunt resistor if the ESR, the open-circuit voltage, and the terminal voltage of the cell were known. If these quantities were known, the current consumption could be

directly determined. This problem merits study because the open-circuit voltage of an active cell cannot be measured directly. In addition, the ESR of a cell is dependent on the state of charge, the state of health, and the temperature of the cell [3]. Thus, these quantities must be estimated before a current estimate can be achieved.

Although current estimation techniques for this application do not appear in the literature, there have been significant contributions in the parameter estimation and mathematical modeling of a lithium battery, as well as detailed work in observer theory which can be utilized to develop a current estimator. Beginning with battery modeling, most models can be classified as electrochemical, thermal, adaptive, or circuit models. Electrochemical models consider the chemical processes occurring inside a cell [4], [5]. These models are accurate, but require detailed parameterization that is often difficult to obtain in practice. Thermal models of the form in [6] can be employed, but more information is required to completely characterize the cell's behavior. Adaptive models can be used to model the cell itself, but, adaptive models are more often used for parameter estimation in the context of a circuit model. Various forms of the Kalman filter are used to this effect in [1], [7]–[10], whereas a proportional-integral observer is used in [11]. Further adaptive techniques such as a Lyapunov-based approach [12], or a recursive least-squares approach [13] are used. Other methods of battery modeling or state of charge estimation range from purely mathematical and established methods, such as that in [14], which uses a modified form of the Peukert equation, to novel and undeveloped methods such as that in [15], which attempts to determine state of charge by applying an external magnetic field.

Circuit models generally lend themselves well to developing control systems for

practical uses of lithium batteries due to their simple parameterization. Most lithium battery circuit models include a state of charge dependent open-circuit voltage term and a series resistance, which can be followed by two parallel RC elements that represent the dynamic behavior of the cell [3], [16]–[20]. Alternatively, three parallel RC elements have been used in an attempt to achieve greater model convergence [21]. These models can be further augmented by considering additional effects such as temperature-dependent self-discharge [22], parameter dependence on state of health [23], or open-circuit voltage hysteresis terms [24]–[29].

Each of these battery models uses cell current as an input in order to estimate the other cell parameters such as state of charge. In this work, it is not presumed that a current measurement is available; thus, none of the models can be applied directly. To remedy this problem, significant work in observer theory is applied which attempts to estimate an output signal when one or more of the input signals are unavailable. These unknown input observers (UIO) have been developed for a broad range of systems. Linear, continuous systems are considered in [30]–[38]. Each of those works only consider systems without a direct feed-through term, but this term is required in all cell models that include a series resistance. Fortunately, this term is included in [39]; however, it is presented in discrete time. Further works consider non-linear systems in order to develop more robust structures at the expense of computational complexity [40]–[44].

This work contributes a practical battery model developed from a survey of the literature, as well as a novel technique by which the current consumption in a battery pack can be determined without the need of any additional current-measuring hardware.

Additionally, the battery model and the current estimation technique are compared with experimental data that demonstrate the accuracy of the model and the estimator. Finally, this work contributes a demonstration of the current estimation technique as employed in a BMS.

The work is organized as follows. In Chapter Two, a model for a lithium battery cell is developed. In Chapter Three, the mathematical model for a UIO is derived and applied to the current estimation problem. Chapter Four details the determination of model parameters. Model validation and experimental results are given in Chapter Five. Chapter Six concludes the work.

CHAPTER TWO: LITHIUM BATTERY MODEL

The problem of developing a practical circuit model for a lithium battery is non-trivial because a battery is an inherently electro-chemical device and exhibits non-linear behaviors that are difficult to capture in a circuit model. Nevertheless, circuit models have been able to achieve sufficient approximations for the dynamics of the lithium battery.

Almost all of the proposed circuit models include an open-circuit voltage that is dependent on the state of charge of the battery and a dynamic system that relates the open-circuit voltage to the measured terminal voltage of the battery. For the purpose of creating a current estimator, an accurate circuit model of a lithium battery cell can be achieved using a second-order RC circuit with a series resistance and two dependent sources describing the open-circuit voltage and the hysteresis voltage. This construction is shown in Figure 2.1. The open-circuit voltage v_{oc} is a non-linear, but monotonically increasing, function of the state of charge soc of the cell. Moreover, the hysteresis voltage v_h is a non-linear function of soc and is dynamically dependent on load current i_l. This circuit model along with relations governing the open-circuit voltage and hysteresis voltage are used to develop a complete set of equations to represent a lithium battery, accounting for various physical phenomena.

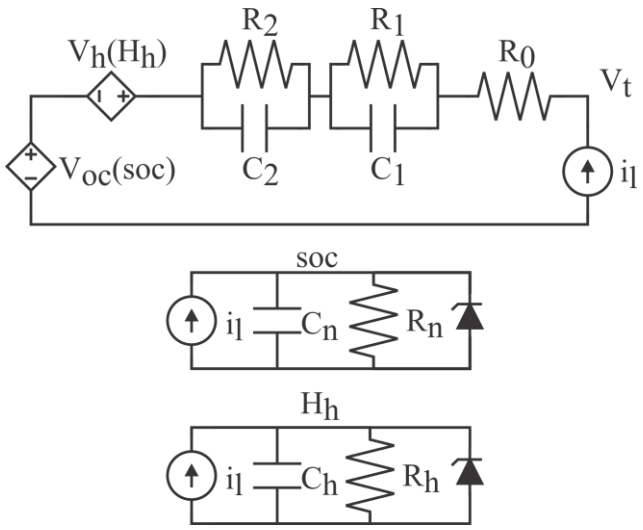

Figure 2.1: Circuit model of a lithium battery cell based on a 2nd order RC design.

A. State of charge

State of charge can be represented as the voltage across a capacitor that represents the battery capacity C_n along with a parallel resistance R_n which represents the self-discharge effect of the battery. The soc represents the ratio of remaining charge in the cell and the total charge capacity of the cell and, thus, must be bounded between zero and unity. Further, the sign convention is defined such that a positive i_l term represents a cell that is charging. These constraints result in the dynamic equation presented below.

$$\dot{soc} = \begin{cases} \frac{i_l}{C_n} - \frac{1}{R_n C_n} soc & 0 < soc < 1 \\ 0 & \text{Otherwise.} \end{cases} \quad (1)$$

For many high-power applications including electric vehicle batteries, the self-discharge is insignificant and can be neglected by setting R_n to an infinite resistance [20]. However,

this will prove to be problematic for the stability of the proposed observer; thus, a large but finite self-discharge resistance term will be used.

A nonlinear relationship exists between soc and open-circuit voltage. It can be approximated as a linear relationship with a constant scale factor α such that

$$v_{oc} - v_{oc_0} = \alpha \cdot soc, 0 < soc < 1, \tag{2}$$

where v_{oc_0} represents the open-circuit voltage that appears on the cell when the cell is discharged to 0% state of charge. In reality, α is moderately state of charge dependent and will be adjusted periodically so that the approximation can remain effective.

B. Hysteresis

Hysteresis refers to the difference in open-circuit voltage in the charging and discharging conditions. Multiple mathematical models have been proposed to capture this effect [24]–[29], but the model from [29] is used in this study due to the computational simplicity and ease of integration into a linear state model. It can be represented by taking the discharge open-circuit voltage and adding a hysteresis term to that voltage to make up the total open-circuit voltage. The total deviation from the discharge v_{oc} curve can be represented as a percent of the maximum voltage deviation for a given soc, where the percent deviation changes with load current. Like the soc term, H_h represents a ratio of present deviation to maximum deviation, and thus it must be bounded between saturation points zero and unity. Further, the hysteresis voltage changes with current; thus, a self-discharge term, R_h, also appears in this equation.

$$\dot{H}_h = \begin{cases} \frac{i_l}{C_h} - \frac{1}{C_h R_h} H_h & 0 < H_h < 1 \\ 0 & \text{Otherwise.} \end{cases} \quad (3)$$

Conveniently, the hysteresis equation takes the same form as the state of charge equation, with C_h representing a capacitor which provides inertia between the charge and discharge hysteresis states. Similar to the state of charge relationship, a state of charge dependent scale factor H_{max} can be used to convert the hysteresis term to a voltage contribution.

$$v_h = H_h H_{max}, \quad 0 < H_h < 1. \quad (4)$$

C. Voltage Relaxation

The terminal voltage of a battery cell which has been under discharge load but is then allowed to rest will increase asymptotically towards the open circuit voltage. This phenomenon has been termed the relaxation effect. It is due, in part, to the surface capacitance of the battery cell, but transient behavior is exhibited at multiple frequencies. It will be represented with two RC circuits placed in series. The RC circuits can be represented using capacitor voltages as state variables.

$$\dot{v_1} = -\frac{1}{R_1 C_1} v_1 + \frac{1}{C_1} i_l, \quad (5)$$

$$\dot{v_2} = -\frac{1}{R_2 C_2} v_2 + \frac{1}{C_2} i_l, \quad (6)$$

where the resistance R_1 and capacitance C_1 represent the fast dynamics of the relaxation effect, and R_2 and C_2 represent the slower dynamics of the relaxation effect. The value of these parameters must be empirically fit to match the response of a particular lithium battery cell.

D. Series Resistance

In addition to transient effects that relate the open-circuit voltage to the terminal voltage, the charge path to the terminals creates a Thévenin resistance between the open-circuit voltage and the terminal voltage.

$$v_0 = R_0 i_l, \tag{7}$$

where R_0 is the internal Thévenin resistance of the cell and v_0 is the voltage drop across that resistance.

E. Terminal Voltage

The terminal voltage can be computed by summing the individual contributions of all of the cell's internal effects.

$$v_t = v_{oc} + v_h + v_1 + v_2 + v_0. \tag{8}$$

F. Nonlinear Effects

The model presented in this work is an approximation of the battery dynamics about a particular state of charge. The battery parameters have each been presented as constants in the battery dynamics. However, in reality, all of these parameters are dependent on one or more other factors. Fortunately, each of these parameters change very slowly with respect to the battery dynamics, and a suitable approximation can be made by considering these parameters as constants in a saturated, but otherwise linear, system and then periodically updating the value of these parameters as they change with state of charge.

The energy capacity of the cell will be represented by the charge stored in the capacitor C_n. This value is dependent on capacity fade [3] and the rate-capacity effect [18], which are two phenomena that reduce the usable current capacity of a cell. The rate-capacity effect does not result in permanent loss of capacity and refers to the fact that a battery will exhibit a smaller effective capacity when discharged or charged at a higher rate of current; thus, it is dependent on the load current of the cell. Moreover, the capacity fade effect is an irreversible effect that refers to the diminishing effective capacity over the lifetime of the cell, which is caused by degradation of the active cell material and is affected by temperature and load current. This variable capacitance can be expressed as

$$C_n = f(i_l)\, soh, \tag{9}$$

where $f(i_l)$ is a non-linear function of load current that represents the rate-capacity effect, and soh is a scale factor that represents the ratio of the actual charge capacity of the cell to the nameplate charge capacity, also known as the state of health of the cell. The state of heath decreases over the lifetime of a cell, and the rate at which this occurs is related to the load current and temperature the cell has experienced, but under normal operating conditions, the state of health decreases very slowly compared to each of the other effects and is considered a constant in this work.

The capacitance C_h represents a capacitor which stores amount of charge required to bring a cell from zero hysteresis voltage to maximum hysteresis voltage. This charge is a fraction of the cell capacity and is experimentally determined.

The H_{max} parameter represents the difference between the open-circuit voltage during a charge cycle and the open-circuit voltage during a discharge cycle. It is experimentally determined as a function of soc.

A relationship between the open-circuit voltage and the state of charge is found by discharging the cell at a sufficiently small current and approximating the open-circuit voltage with the terminal voltage. The value of α is directly determined from (2) by solving for α and expressing both the open-circuit voltage and α itself as a function of state of charge and temperature.

Moreover, the relaxation effect has been experimentally determined to depend on the state of charge of the cell [18], [20], and, as a result, the values of R_2, R_1, C_1, and C_2 are experimentally determined as functions of soc. The internal resistance term, R_0, exhibits strong temperature dependence, moderate state of heath dependence, and weak state of charge dependence [16]. It is represented in this model as a function of both temperature and state of charge, with state of health appearing as a supplied constant.

Several of the cell parameters are functions of temperature; however, temperature is not included as an input to a state model of this system due to its highly nonlinear relationship with each of the parameters. It will be treated as an input to the functions which update the cell parameters.

G. Linear State Model

The circuit model, less the limiting diodes, can be represented as a linear state-variable model with four state variables: soc, H_h, v_1, and v_2. The state model shown below will act as the basis for the development of a current estimator.

$$\dot{x}(t) = \begin{bmatrix} -\frac{1}{R_n C_n} & 0 & 0 & 0 \\ 0 & -\frac{1}{R_h C_h} & 0 & 0 \\ 0 & 0 & -\frac{1}{R_1 C_1} & 0 \\ 0 & 0 & 0 & -\frac{1}{R_2 C_2} \end{bmatrix} x(t) + \begin{bmatrix} \frac{1}{C_n} \\ \frac{1}{C_h} \\ \frac{1}{C_1} \\ \frac{1}{C_2} \end{bmatrix} w(t). \quad (10)$$

The output equation is given by

$$y(t) = [\alpha \quad H_{max} \quad 1 \quad 1]x(t) + \mathrm{R}_0 w(t), \quad (11)$$

where $y(t) = v_t - v_{oc_0}$, and $w(t) = i_l(t)$. The limiting diodes do not appear in this expression but are implemented as saturated integrators.

CHAPTER THREE: UNKNOWN INPUT OBSERVER

A. Derivation of the Unknown Input Observer

The derivation of the unknown input observer presented here closely follows the derivation as presented in [39], with the exception that this derivation considers a continuous-time system. A continuous, linear, time-invariant system can be expressed as shown.

$$\dot{x}(t) = \boldsymbol{A}x(t) + \boldsymbol{B}w(t),\ t \geq t_0, \tag{12}$$

$$y(t) = \boldsymbol{C}x(t) + \boldsymbol{D}w(t),$$

where $x \in \mathbb{R}^n$ is the state of the system, $w \in \mathbb{R}^m$ is the unknown input to the system, and $y \in \mathbb{R}^p$ is the measured output of the system. The matrices $\boldsymbol{A}$, $\boldsymbol{B}$, $\boldsymbol{C}$, and $\boldsymbol{D}$ are real, constant, matrices of appropriate dimensions.

A full-order unknown-input state observer for this system can be described by

$$\dot{z}(t) = \boldsymbol{N}z(t) + \boldsymbol{L}y(t),\ t \geq t_0, \tag{13}$$

$$\hat{x}(t) = z(t) + \boldsymbol{E}y(t),$$

where $\hat{x} \in \mathbb{R}^n$ is the estimated state of the system, and $\boldsymbol{N}$, $\boldsymbol{L}$, and $\boldsymbol{E}$ are constant, real matrices of appropriate dimensions. Necessarily, this state observer must estimate the state of the system with no knowledge of the input since it is unknown or otherwise unmeasureable. This observer is required to suitably estimate the state of the system such

that the estimate of the state asymptotically converges to the true state. This requirement can be described with an error vector

$$e(t) = \hat{x}(t) - x(t), \tag{14}$$

where the observer exists if and only if the matrices $\boldsymbol{N}$, $\boldsymbol{L}$, and $\boldsymbol{E}$ can be found such that

$$\lim_{t\to\infty} e(t) = 0. \tag{15}$$

Theorem 1: The unknown input observer (13) for the system (12) exists if and only if the following conditions are satisfied:

1) $\boldsymbol{N}$ is Hurwitz stable.
2) $\boldsymbol{LC} - (\boldsymbol{I_n} - \boldsymbol{EC})\boldsymbol{A} + \boldsymbol{N} - \boldsymbol{NEC} = 0$.
3) $\boldsymbol{LD} - (\boldsymbol{I_n} - \boldsymbol{EC})\boldsymbol{B} = 0$.
4) $\boldsymbol{ED} = 0$.

Proof: By substituting the system and the observer model into the error vector equation, it can be shown that

$$\begin{aligned}
\dot{e}(t) &= \dot{\hat{x}}(t) - \dot{x}(t) \\
&= (\dot{z}(t) + \boldsymbol{E}\dot{y}(t)) - \dot{x}(t) \\
&= (\boldsymbol{N}z(t) + \boldsymbol{L}y(t)) + \boldsymbol{E}\dot{y}(t) - \boldsymbol{A}x(t) - \boldsymbol{B}w(t) \\
&= \boldsymbol{N}\big(\hat{x}(t) - \boldsymbol{E}y(t)\big) + \boldsymbol{L}y(t) + \boldsymbol{E}\dot{y}(t) - \boldsymbol{A}x(t) - \boldsymbol{B}w(t) \\
&= \boldsymbol{N}\hat{x}(t) - \boldsymbol{A}x(t) + (\boldsymbol{L} - \boldsymbol{NE})y(t) + \boldsymbol{E}\dot{y}(t) - \boldsymbol{B}w(t)
\end{aligned}$$

$$= \boldsymbol{N}\hat{x}(t) - \boldsymbol{A}x(t) + (\boldsymbol{L} - \boldsymbol{NE})\big(\boldsymbol{C}x(t) + \boldsymbol{D}w(t)\big) + \boldsymbol{E}\big(\boldsymbol{C}\dot{x}(t) + \boldsymbol{D}\dot{w}(t)\big) - \boldsymbol{B}w(t)$$

$$= \boldsymbol{N}\hat{x}(t) - \boldsymbol{A}x(t) + (\boldsymbol{LC} - \boldsymbol{NEC})x(t) + (\boldsymbol{LD} - \boldsymbol{NED})w(t) + \boldsymbol{EC}\dot{x}(t) - \boldsymbol{B}w(t) + E\boldsymbol{D}\dot{w}(t)$$

$$= \boldsymbol{N}\hat{x}(t) - \boldsymbol{A}x(t) + (\boldsymbol{LC} - \boldsymbol{NEC})x(t) + (\boldsymbol{LD} - \boldsymbol{NED})w(t) + \boldsymbol{ECA}x(t) + EC\boldsymbol{B}w(t) - \boldsymbol{B}w(t) + E\boldsymbol{D}\dot{w}(t)$$

$$= \boldsymbol{N}\hat{x}(t) + (\boldsymbol{LC} - \boldsymbol{NEC})x(t) + (\boldsymbol{LD} - \boldsymbol{NED})w(t) + (\boldsymbol{EC} - \boldsymbol{I_n})\boldsymbol{A}x(t) + (EC - \boldsymbol{I_n})\boldsymbol{B}w(t) + E\boldsymbol{D}\dot{w}(t)$$

$$= \boldsymbol{N}\hat{x}(t) + (\boldsymbol{LC} - \boldsymbol{NEC} + (\boldsymbol{EC} - \boldsymbol{I_n})\boldsymbol{A})x(t) + (\boldsymbol{LD} - \boldsymbol{NED} + (EC - \boldsymbol{I_n})\boldsymbol{B})w(t) + E\boldsymbol{D}\dot{w}(t)$$

$$= \boldsymbol{N}\hat{x}(t) + [\boldsymbol{LC} - (\boldsymbol{I_n} - \boldsymbol{EC})\boldsymbol{A} - \boldsymbol{NEC}]x(t) + [\boldsymbol{LD} - (I_n - EC)\boldsymbol{B} - \boldsymbol{NED}]w(t) + E\boldsymbol{D}\dot{w}(t)$$

$$= \boldsymbol{N}e(t) + [\boldsymbol{LC} - (\boldsymbol{I_n} - \boldsymbol{EC})\boldsymbol{A} + \boldsymbol{N} - \boldsymbol{NEC}]x(t) + [\boldsymbol{LD} - (I_n - \boldsymbol{EC})\boldsymbol{B} - \boldsymbol{NED}]w(t) + \boldsymbol{ED}\dot{w}(t).$$

By inspection, (15) holds if and only if the error equation updates such that $\dot{e}(t) = \boldsymbol{N}e(t)$, with $\boldsymbol{N}$ Hurwitz. Therefore, from this equation, one can conclude that the observer exists if and only if each of state and input coefficients are zero and the error vector

coefficient $\boldsymbol{N}$ is Hurwitz. Hence, the four presented conditions are necessary and sufficient.

Remark 1: For a single-input, single-output (SISO) system, as is the case for the battery model, the $\boldsymbol{D}$ matrix is a non-zero scalar and, thus, has full rank. The conditions of Theorem 1 can be simplified if $\boldsymbol{D}$ has full rank because the only $\boldsymbol{E}$ that fulfils condition 4) is the zero matrix. This leads to the following corollary to Theorem 1.

Corollary 1: If the $\boldsymbol{D}$ matrix has full rank, the unknown input observer (13) for the system (12), exists if and only if the following conditions are satisfied:

1) $\boldsymbol{N}$ is Hurwitz stable.
2) $\boldsymbol{LC} - \boldsymbol{A} + \boldsymbol{N} = 0$.
3) $\boldsymbol{LD} - \boldsymbol{B} = 0$.

From these three conditions, the unknown matrices can be determined. Condition 2) can be solved directly.

$$\boldsymbol{N} = \boldsymbol{A} - \boldsymbol{LC}, \tag{16}$$

where $\boldsymbol{A} - \boldsymbol{LC}$ must be asymptotically stable. Similarly, condition 3) implies

$$\boldsymbol{LD} = \boldsymbol{B}. \tag{17}$$

For the battery model (a SISO system), the $\boldsymbol{D}$ matrix is invertible. This allows a solution for $\boldsymbol{L}$ to follow directly from (17) where

$$\boldsymbol{L} = \boldsymbol{B}\boldsymbol{D}^{-1}. \tag{18}$$

It is also of interest to find an estimation of the unknown input vector, $\widehat{w}(t)$. An expression for $\widehat{w}(t)$ follows directly from the system output equation, where the estimated input and state is used in place of the true input and state. If $\boldsymbol{D}$ is invertible and $\boldsymbol{E} = 0$, then $\widehat{w}(t)$ can be expressed directly as shown.

$$\begin{aligned} \widehat{w}(t) &= \boldsymbol{D^{-1}}\big(y(t) - \boldsymbol{C}\hat{x}(t)\big), \\ &= \boldsymbol{D^{-1}}[y(t) - \boldsymbol{C}(z(t) + \boldsymbol{E}y(t))], \\ &= \boldsymbol{D^{-1}}(y(t) - \boldsymbol{C}z(t)). \end{aligned} \tag{19}$$

B. Presentation of the Current Estimator

A full-order unknown input observer of the form presented in (13) exists for this system if the unknown matrices can be found and the conditions from Corollary 1 are satisfied. For the battery system,

$$\boldsymbol{L} = \begin{bmatrix} \frac{1}{R_0 C_n} & \frac{1}{R_0 C_h} & \frac{1}{R_0 C_1} & \frac{1}{R_0 C_2} \end{bmatrix}^T. \tag{20}$$

$$\boldsymbol{N} = \begin{bmatrix} -\frac{1}{R_n C_n} & 0 & 0 & 0 \\ 0 & -\frac{1}{R_h C_h} & 0 & 0 \\ 0 & 0 & -\frac{1}{R_1 C_1} & 0 \\ 0 & 0 & 0 & -\frac{1}{R_2 C_2} \end{bmatrix} - \begin{bmatrix} \frac{1}{R_0 C_n} \\ \frac{1}{R_0 C_h} \\ \frac{1}{R_0 C_1} \\ \frac{1}{R_0 C_2} \end{bmatrix} \begin{bmatrix} \alpha \\ H_{max} \\ 1 \\ 1 \end{bmatrix}^T. \tag{21}$$

$$\boldsymbol{E} = 0. \tag{22}$$

The current estimator itself would take the form presented in (19). Substituting the battery parameters, the expression for current estimation becomes

$$\hat{w}(t) = \frac{1}{R_0}(y(t) - \begin{bmatrix}\alpha & H_{max} & 1 & 1\end{bmatrix} z(t)). \tag{23}$$

C. Existence of the Current Estimator

It has been shown that if an unknown input observer of the form described in (13) exists for the lithium battery system, then the observer is uniquely determined. What remains is to show that the observer exists for the dynamics of the battery model. This amounts to satisfying the first condition of Corollary 1, which states that $\boldsymbol{N}$ must be Hurwitz stable. In reality, however, this observer is an approximation of a nonlinear system, and the system parameters which make up the $\boldsymbol{N}$ matrix change their values nonlinearly with soc, T, and i_l. Thus, it must be shown that the system will remain stable in the context of the nonlinear behavior.

One possible method for reconciling this nonlinear behavior is to consider the system as a piecewise-linear model as in [45], where there exist a discrete set of regions in state space for which particular $\boldsymbol{N}$ matrices apply. This lends itself well to a non-interpolative lookup table implementation in a microcontroller. However, empirical analysis has shown that the number of discrete regions required in this scheme is not feasible for a microcontroller implementation. As such, an interpolative lookup table scheme will be used, and the piecewise-linear model is insufficient.

It is also possible to delay the re-computation of the $\boldsymbol{N}$ matrix such that it only updates its particular value at a frequency much slower than the sampling frequency. This will allow the system to be approximated as a linear system such that stability can be shown if all possible $\boldsymbol{N}$ matrices are Hurwitz**,** or equivalently if all of the Eigenvalues of $\boldsymbol{N}$ are negative for each possible $\boldsymbol{N}$. The parameters making up the **N** matrix are most

strongly dependent on state of charge, then temperature, and lastly, load current. The Eigenvalue analysis of Figure 3.1 shows that the largest Eigenvalue is very weakly dependent on temperature, and more strongly dependent on state of charge and load current. In all cases, the largest Eigenvalue of **N** is negative, which implies that the system will be stable.

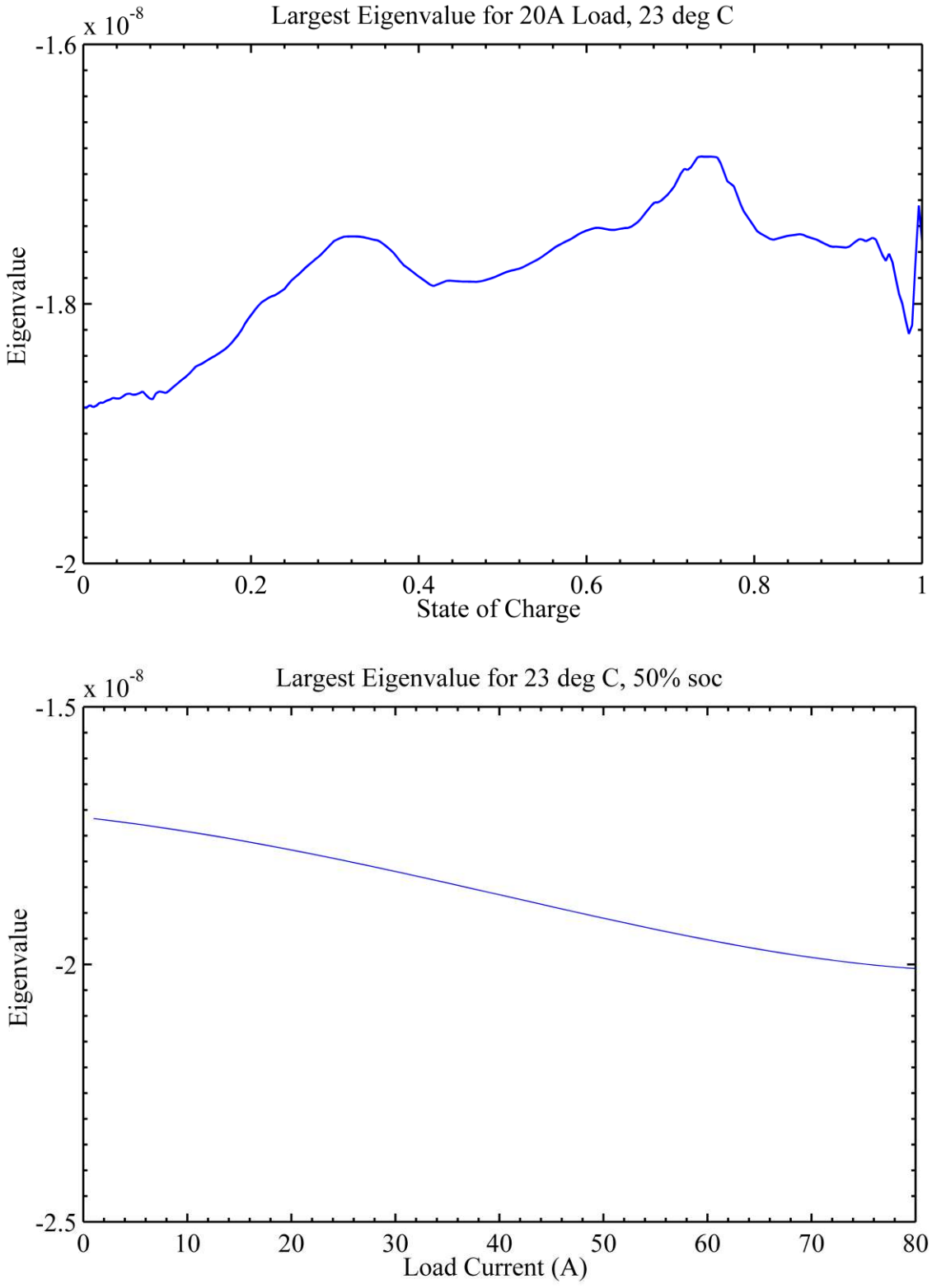

Figure 3.1: Eigenvalue Analysis. Across the full range of states of charge, cell temperatures, and load currents, all of the unknown input observer's Eigenvalues are negative.

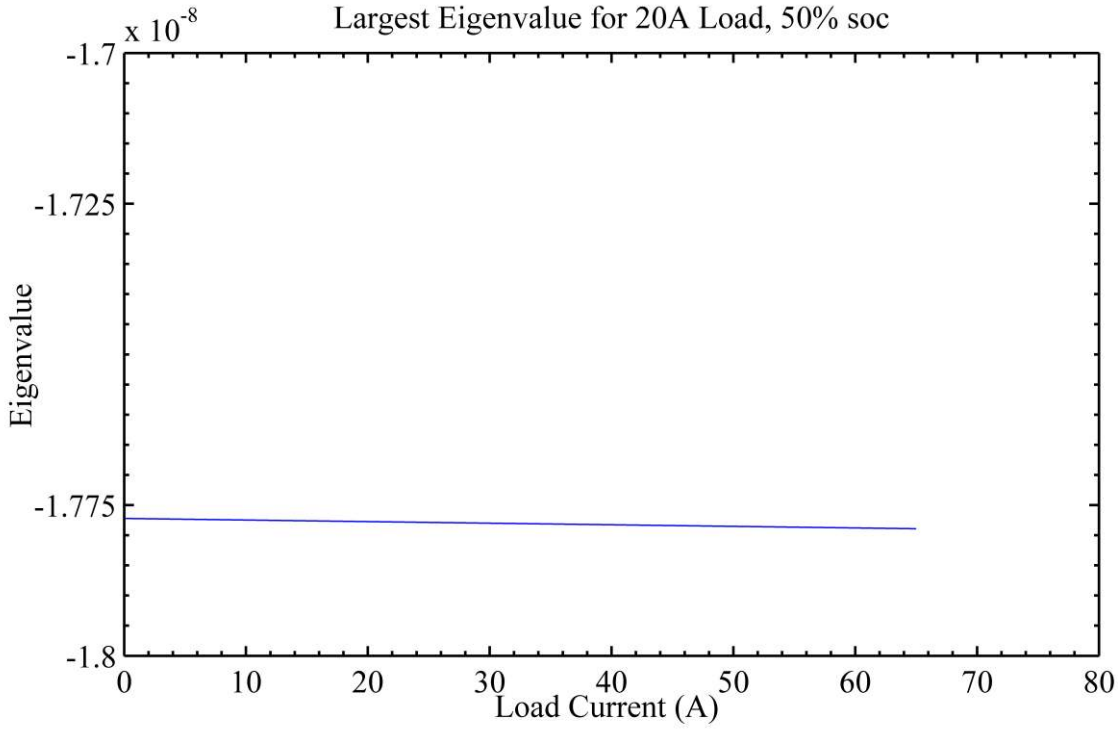

Figure 3.1, Cont'd: Eigenvalue Analysis. Across the full range of states of charge, cell temperatures, and load currents, all of the unknown input observer's Eigenvalues are negative.

D. Discretization of the Current Estimator

Any microcontroller implementation of an unknown input observer will necessarily exist in discrete time, thus it is necessary to transform the continuous time model into an equivalent discrete time model so that the system can be implemented on a microcontroller. The results from [46] can be used to complete this equivalence transformation.

$$\boldsymbol{A_d} = e^{\boldsymbol{A}T_s}, \tag{24}$$

$$\boldsymbol{B_d} = \int_0^{T_s} e^{\boldsymbol{A}t}\boldsymbol{B}\, dt, \tag{25}$$

$$\boldsymbol{C_d} = \boldsymbol{C}, \tag{26}$$

$$\boldsymbol{D_d} = \boldsymbol{D}, \tag{27}$$

where T_s is the sampling period. The transformation yields the cell model matrices

$$\boldsymbol{A_d} = \begin{bmatrix} e^{-\frac{T_s}{R_n C_n}} & 0 & 0 & 0 \\ 0 & e^{-\frac{T_s}{R_h C_h}} & 0 & 0 \\ 0 & 0 & e^{-\frac{T_s}{R_1 C_1}} & 0 \\ 0 & 0 & 0 & e^{-\frac{T_s}{R_2 C_2}} \end{bmatrix}, \text{ and} \tag{28}$$

$$\boldsymbol{B_d} = \begin{bmatrix} R_n - R_{n_b} e^{-\frac{T_s}{R_n C_n}} \\ R_h - R_h e^{-\frac{T_s}{R_h C_h}} \\ R_1 - R_1 e^{-\frac{T_s}{R_1 C_1}} \\ R_2 - R_2 e^{-\frac{T_s}{R_2 C_2}} \end{bmatrix}. \tag{29}$$

The observer matrices can be transformed in a similar manner into their discrete-time counterparts. The results of the transformation are shown below.

$$\boldsymbol{L_d} = \begin{bmatrix} \frac{R_n}{R_0}\left(1 - e^{-\frac{T_s}{R_n C_n}}\right) \\ \frac{R_h}{R_0}\left(1 - e^{-\frac{T_s}{R_h C_h}}\right) \\ \frac{R_1}{R_0}\left(1 - e^{-\frac{T_s}{R_1 C_1}}\right) \\ \frac{R_2}{R_0}\left(1 - e^{-\frac{T_s}{R_2 C_2}}\right) \end{bmatrix}. \tag{30}$$

$$\boldsymbol{N_d} = \begin{bmatrix} e^{-\frac{T_S}{R_n C_n}} & 0 & 0 & 0 \\ 0 & e^{-\frac{T_S}{R_h \mathrm{C_h}}} & 0 & 0 \\ 0 & 0 & e^{-\frac{T_S}{R_1 C_1}} & 0 \\ 0 & 0 & 0 & e^{-\frac{T_S}{R_2 C_2}} \end{bmatrix} - \begin{bmatrix} \frac{R_b}{R_0}\left(1 - e^{-\frac{T_S}{R_n C_n}}\right) \\ \frac{R_b}{R_0}\left(1 - e^{-\frac{T_S}{R_h C_h}}\right) \\ \frac{R_1}{R_0}\left(1 - e^{-\frac{T_S}{R_1 C_1}}\right) \\ \frac{R_2}{R_0}\left(1 - e^{-\frac{T_S}{R_2 C_2}}\right) \end{bmatrix} \begin{bmatrix} \alpha \\ H_{max} \\ 1 \\ 1 \end{bmatrix}^{\mathrm{T}}. \quad (31)$$

$$\boldsymbol{E_d} = 0. \quad (32)$$

The equation for the unknown input observer itself is a discrete analog to the continuous version derived in this work. The discrete version is derived in [39] and is presented here for convenience.

$$z[k+1] = \boldsymbol{N_d} z[k] + \boldsymbol{L_d} y[k], \quad (33)$$

$$\hat{x}[k] = z[k] + \boldsymbol{E_d} y[k], \text{ for } k \geq 0.$$

The output equation also takes an analogous form.

$$\widehat{w}[k] = \boldsymbol{D_d^{-1}}(y[k] - \boldsymbol{C_d} z[k]). \quad (34)$$

CHAPTER FOUR: DETERMINATION OF MODEL PARAMETERS

The model parameters are experimentally determined by conducting a series of tests on a sample 20-Ah prismatic $LiFePO_4$ cell. A pulsed discharge test is conducted on the cell starting from a maximum open circuit voltage, defined in the cell datasheet as the 100% state of charge point. A 50% duty cycle, 30 minute period square-wave current is drawn from the cell until 0% state of charge is reached. A current magnitude of 4 A is used, and 0% state of charge is defined for a particular open-circuit voltage specified in the cell datasheet. This test is followed by a pulsed charge test with the same charging schedule, and the cell parameters are determined by appropriately fitting the collected test data. The cell parameters are provided in Table 4.1, and the test data appears in Figure 4.1. This test is followed by a pulsed charge test with the same charging schedule. From the results of these tests, several of the parameters are determined using the following procedures.

TABLE 4.1
Cell Parameters

Symbol	Parameter	Value
v_{oc_0}	Voltage at 0% *soc*	2.7500 V
$v_{oc_{100}}$	Voltage at 100% *soc*	3.6000 V
C_n	Nominal Capacity	72000 F
C_h	Hysteresis Capacity	15120 F
soh	State of Health	94.9%
T_{amb}	Ambient Temperature	23℃
T_{gain}	Temperature Gain	0.05
R_n	Self-discharge Resistance	10000 Ω
R_h	Self-discharge Resistance	10000 Ω
C_1	Fast Capacitance at 50% *soc*	28000 F
C_2	Slow Capacitance at 50% *soc*	300000 F
R_1	Fast Resistance at 50% *soc*	2.132 m Ω
R_2	Slow Resistance at 50% *soc*	2.440 m Ω

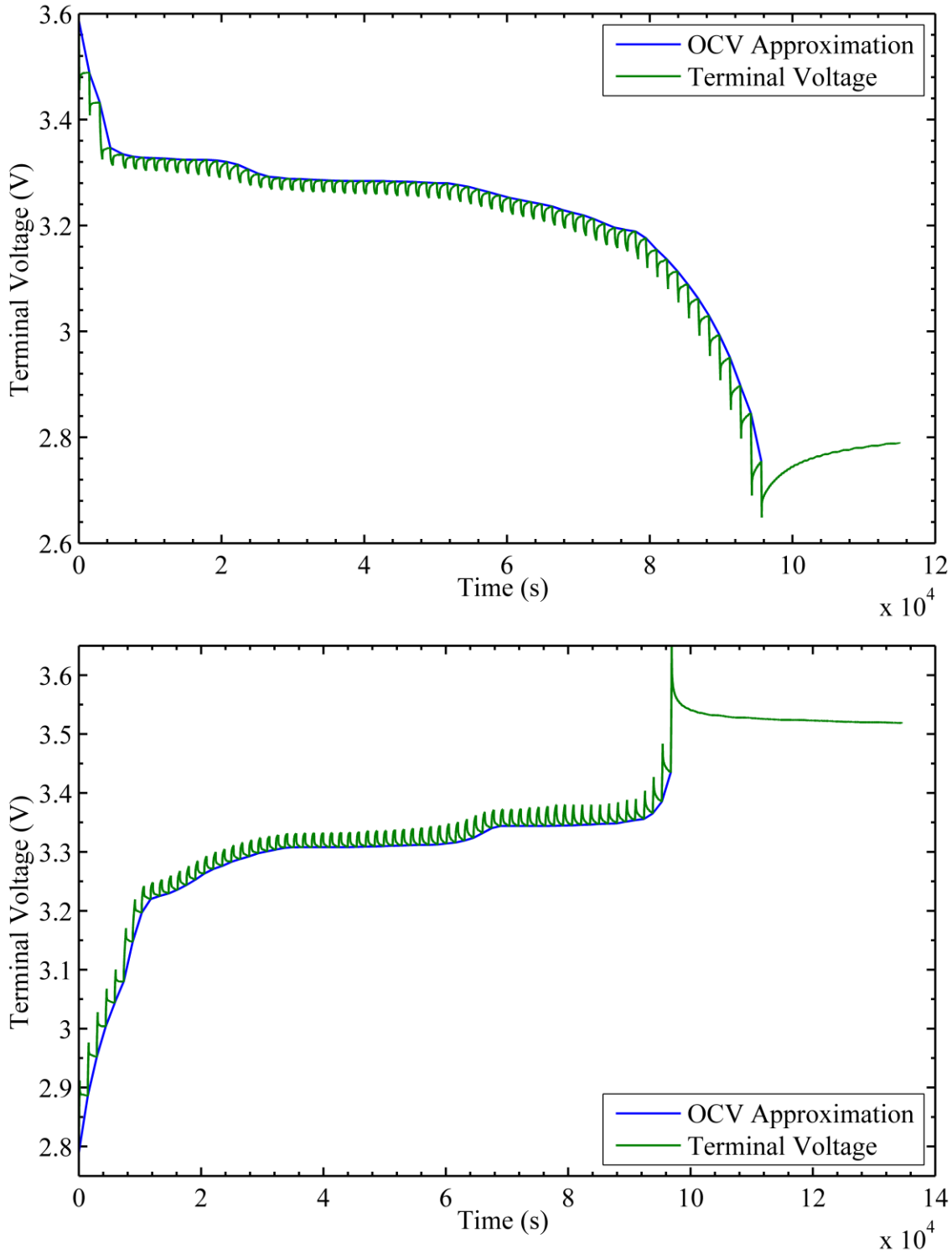

Figure 4.1: Open circuit voltage characteristics of the LiFePO4 cell. The open circuit voltage is measured by completing a full charge and discharge cycle with intermittent rest periods during which the open circuit voltage can be approximated as the terminal voltage.

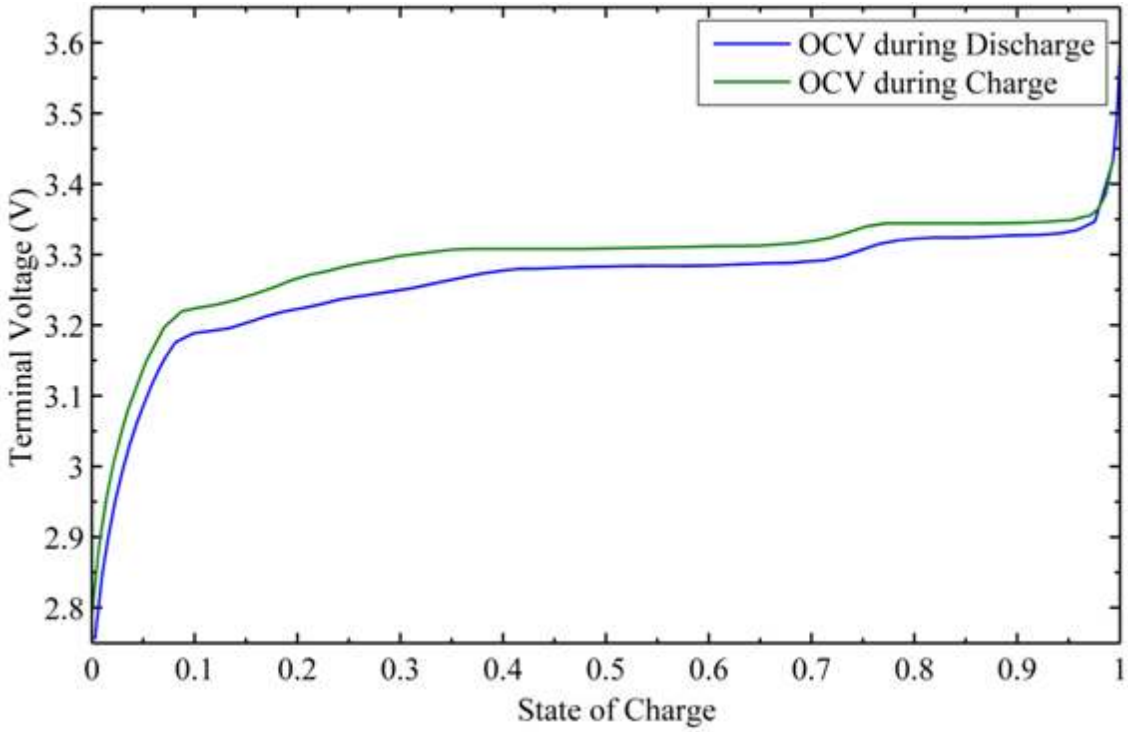

Figure 4.1, Cont'd: Open circuit voltage characteristics of the LiFePO4 cell. The open circuit voltage is measured by completing a full charge and discharge cycle with intermittent rest periods during which the open circuit voltage can be approximated as the terminal voltage.

A. Determination of nominal capacity

The parameter 'C_n' represents a capacitor that holds the nominal energy capacity, Q_n, of the cell. If the cell is at a 100% state of health, Q_n is the integral of current from 100% state of charge to 0% state of charge, and $C_n = Q_n$ because state of charge is defined as a voltage ranging from 0 V to 1 V. The specific value for C_n is given in Table 4.1. It should be noted that the effects of the rate-capacity effect are also included. This effect is found by repeatedly completing a full discharge test for several rates of discharge current and obtaining a ratio of achieved capacity to nominal capacity

for each current. The data is then fit using a polynomial model, and the resultant plot is given in Figure 4.2.

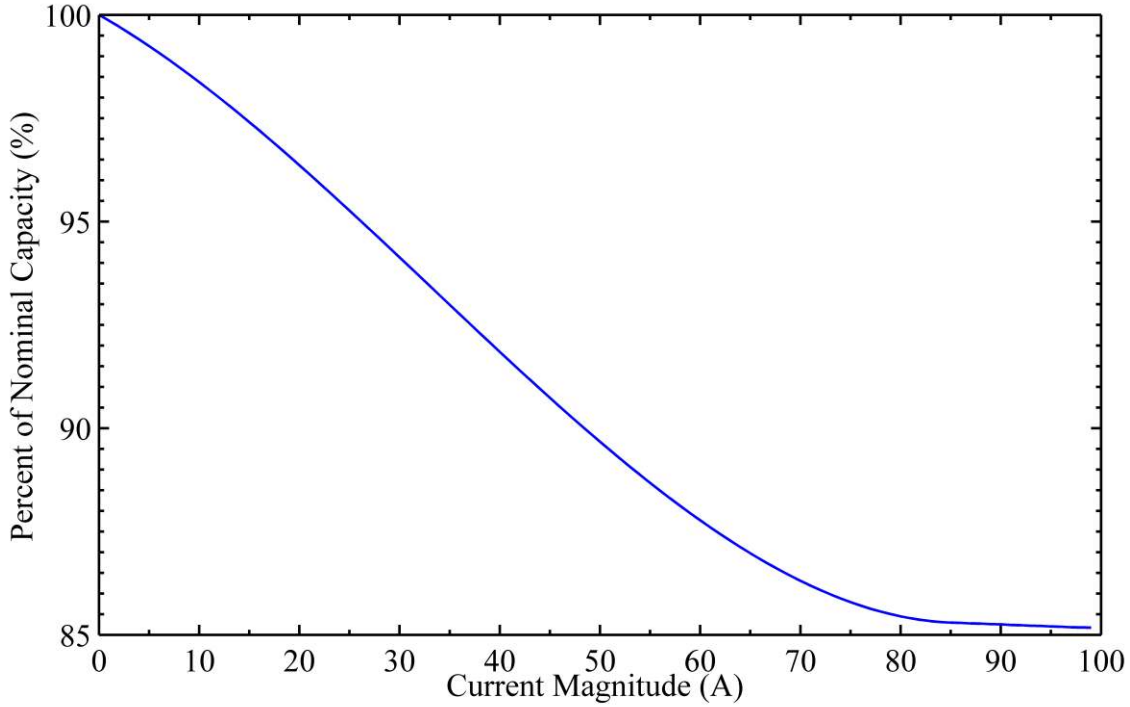

Figure 4.2: The rate-capacity effect is a reversible effect wherein cells cycled at higher rates exhibit a lower energy storage capacity.

B. Determination of Hysteresis Voltage

The parameter 'H_{max}' represents the deviation between the open-circuit voltage found in the charge test, and the open-circuit voltage found in the discharge test. Figure 4.1 demonstrates that the open-circuit voltage can be found by taking the peak values of the collected voltage data, which represents times at which the cell is at rest and the terminal voltage can be approximated as equal to the open-circuit voltage. The relationship between H_{max} and the state of charge is found by taking the difference of the open-circuit voltage measurements for a charge and discharge cycle, and plotting the

result as a function of the state of charge. The results of this procedure are shown in Figure 4.3.

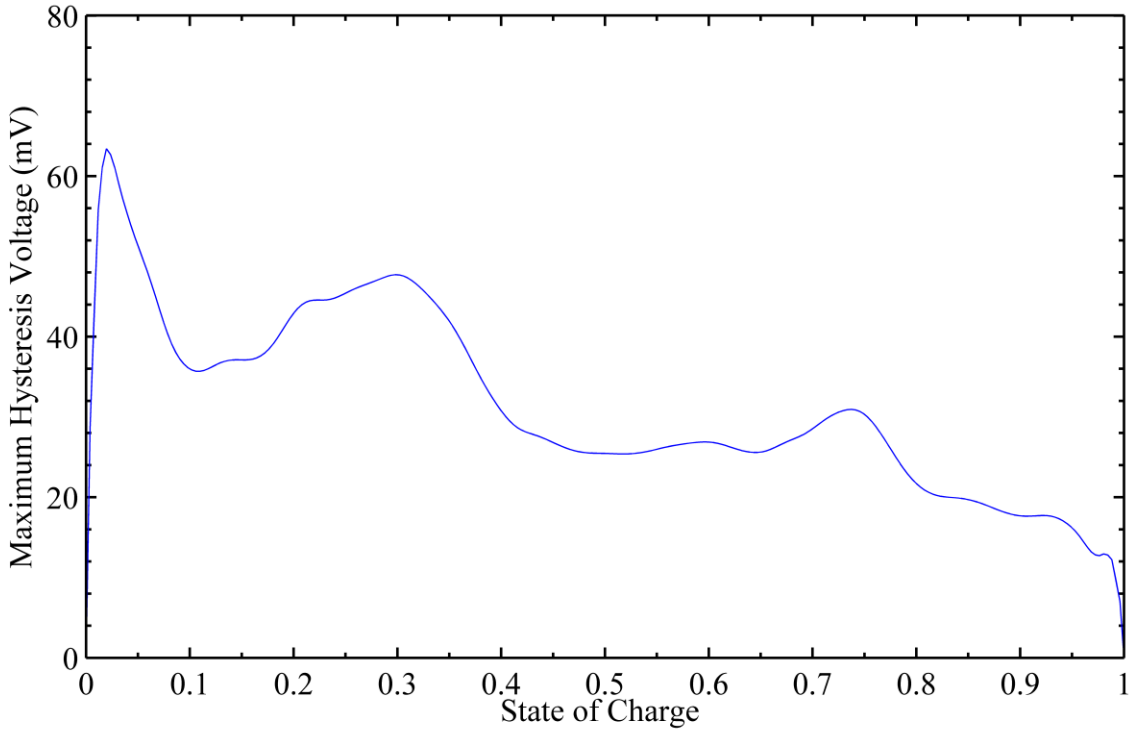

Figure 4.3: Maximum hysteresis voltage as a function of state of charge.

C. Determination of the State of Charge Scale Factor

The parameter 'α' is found from the open-circuit voltage curve during the discharge test, and is shown in Figure 4.4. The effects of temperature are also taken into consideration in the open-circuit voltage curve. This is achieved by using a second table which gives a voltage correction per deviation in temperature from an ambient temperature, T_{amb}, across all states of charge. This effect is small, and requires performing a series of discharge tests in a temperature-controlled environment. As a

result, data from the application guide for the cell [47] is used to characterize this effect. The data is shown in Figure 4.5.

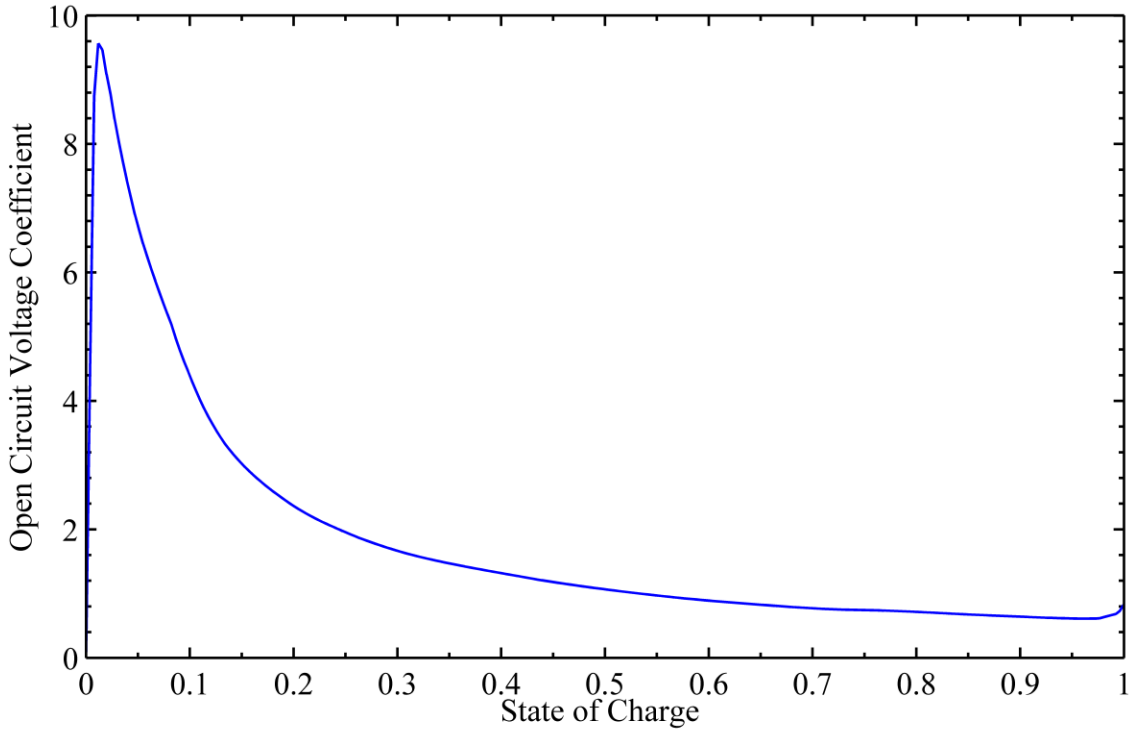

Figure 4.4: The open circuit voltage coefficient, α, appropriately scales the state of charge to the open-circuit voltage.

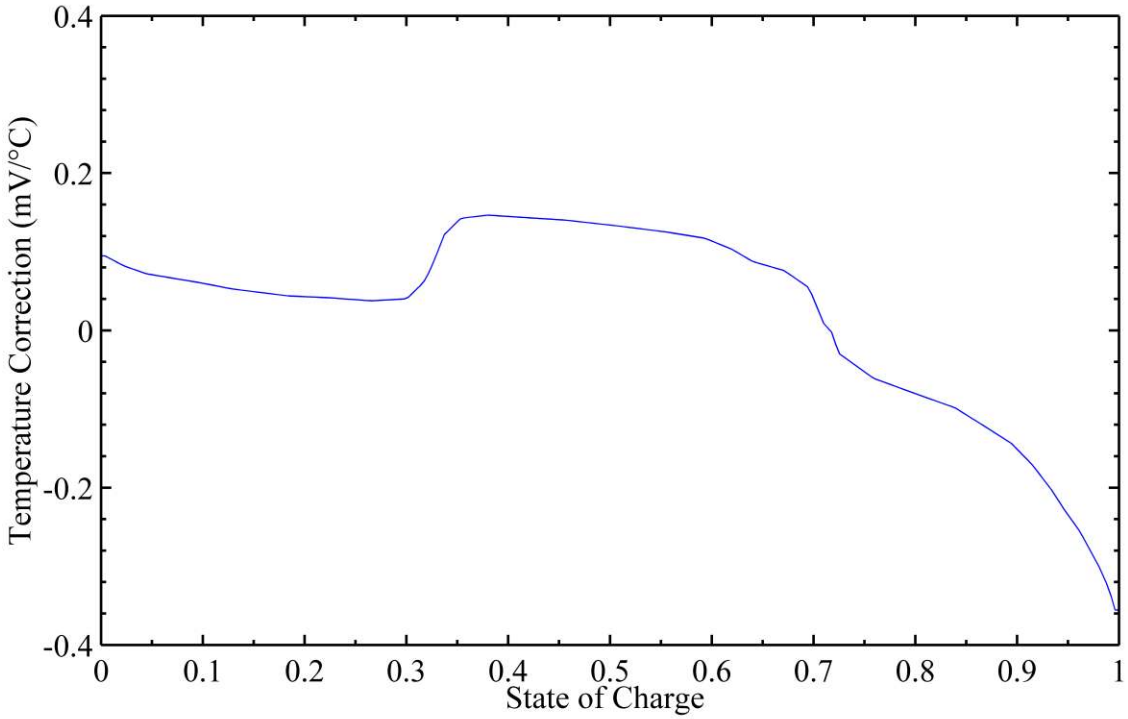

Figure 4.5: Temperature correction for the open circuit voltage.

D. Determination of Internal Resistance

The parameter 'R_0' is also found directly from the pulsed-discharge test. On the rising and falling edge of the current waveform, the measured terminal voltage instantaneously jumps. This voltage jump divided by the current jump yields the DC resistance, which can be computed over the range of states of charge and is shown in Figure 4.6. DC resistance is calculated in this manner in the literature, namely in [16]. However, this method is inaccurate because the DC resistance term is also heavily dependent on temperature. Using the cell R_0 data collected in [47], it was discovered that the DC resistance could be well-approximated by an exponential normalized about a reference ambient temperature such that

$$R_0 = R_{0_{Tamb}} * e^{-T_{gain}*(T_k - T_{amb})}, \quad (35)$$

where the determined values of T_{gain} and T_{amb} are shown in Table 4.1. T_{amb} was simply defined by convention and T_{gain} was determined by using a least-squares parameter fit with the proposed exponential curve.

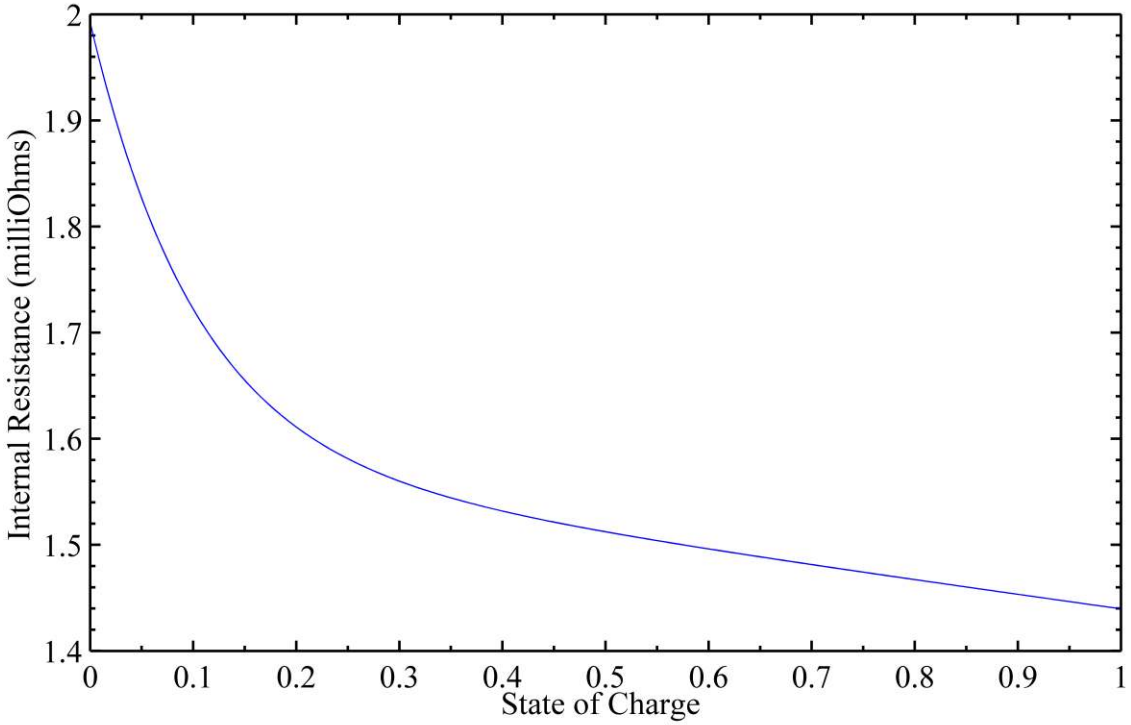

Figure 4.6: Internal Resistance, R_0.

E. Determination of Relaxation Parameters

The resistances $R_1$and R_2, and the capacitances C_1 and C_2, are the parameters that characterize the relaxation effect. During the full discharge tests, there were several periods where the cell was allowed to rest. The time from the beginning of the resting period until the end of the resting period formed a terminal voltage relaxation curve, and the negative of this curve lends itself to a double exponential fit of the form

$$v(t) = ae^{bt} + ce^{dt} + r, \tag{36}$$

where, in this case, this voltage relaxation curve lends itself to matching the transience of a 2nd order RC circuit where

$$v(t) = i_0 R_1 e^{\frac{t}{R_1 C_1}} + i_0 R_2 e^{\frac{t}{R_2 C_2}} + R_0. \tag{37}$$

The relaxation curves, with the R_0 contribution removed, were fit to a double exponential over the entire range of state of charge using the curve fitting function 'fit' within MATLAB. The resulting coefficients were used to solve for the individual $R_2, R_1, C_1,$ and C_2 values. These parameters were fit to a polynomial over the range of states of charge. The results are presented in Figure 4.7.

.

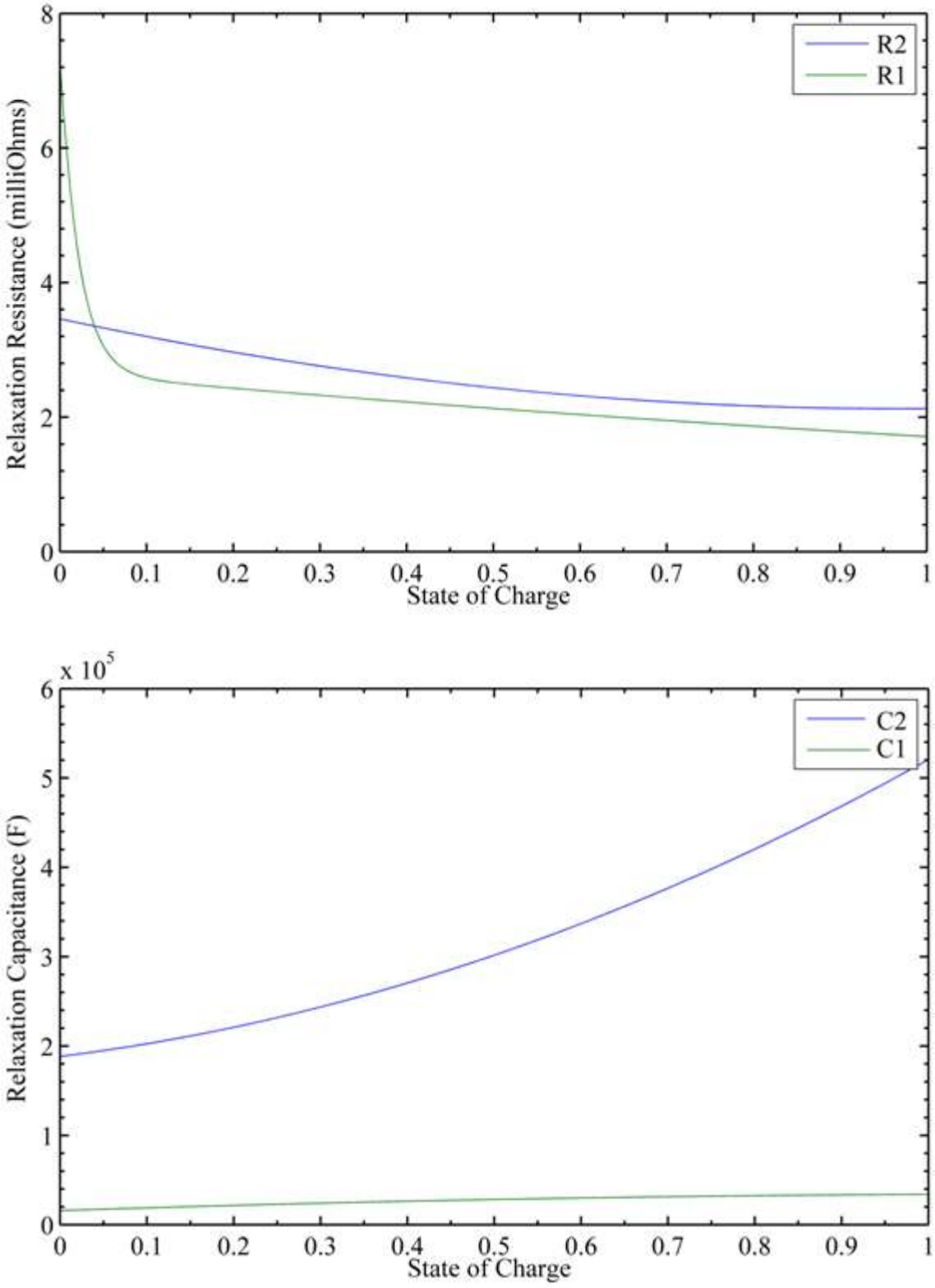

Figure 4.7: Relaxation parameters: R_1, R_2, C_1, and C_2.

F. Determination of the Hysteresis Constant

An additional test was required in order to determine the parameter C_h. This parameter denotes a capacitor that stores the amount of charge required to move the cell from the discharge v_{oc} curve to the charge v_{oc} curve. It represents the inertia of hysteresis term, where a large C_h corresponds to slow and sluggish changes in the hysteresis voltage level. To determine this parameter, a partial discharge-charge cycle was recorded, and the change in state of charge required to transition from the discharge v_{oc} curve to the charge v_{oc} curve was recorded. The result of the test is shown in Figure 4.8 with the computed C_h appearing in Table 4.1. Although the test agreed with the hysteresis model in a practical sense, the test indicated that the hysteresis model adopted in this work bears some differences to the physical hysteresis curve. In particular, the hysteresis model assumes a constant rate of change of the hysteresis voltage, when in reality, the hysteresis voltage changes more slowly as it approaches its maximum or minimum limit. However, due to the relatively small impact of the hysteresis term on the model, noting that several models in the literature ignore the hysteresis effect altogether [3], [16]–[20], and noting the fact that a more accurate model would be inherently non-linear and thus difficult to model in this context, the inaccuracy will be ignored. Finally, an assumption was made that C_h can be modeled as a fixed fraction of C_n. However, this assumption implies that there is no relationship between Q_h and the state of charge of the cell. This effect is not well-explored, but the results of [27] imply this assumption is, at least, a reasonable approximation.

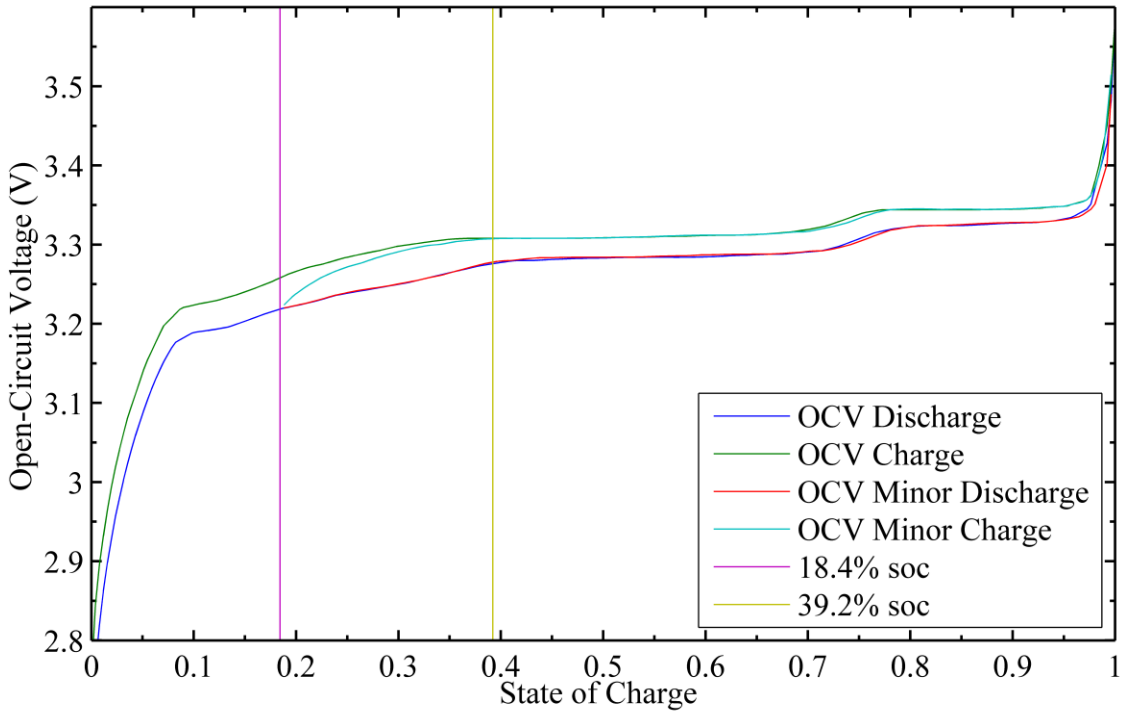

Figure 4.8: Comparison of a full cell cycle and a minor cell cycle shows that approximately 20% of the capacity of the cell is required in order to transition from the discharge open circuit voltage to the charge open circuit voltage.

G. Determination of the Self-Discharge Constant

The value of the constant R_n represents the self-discharge resistance of the cell. It can be found by measuring the state of charge of a cell at rest over a period of several days or months. The difference in stored energy over the difference in time is the average leakage power such that

$$\frac{Q_{final}-Q_{initial}}{\Delta t} = \frac{v_{nom}^2}{R_n}. \tag{38}$$

The value of R_n was calculated using data collected in [46], and the result appears in Table 4.1. Note, however, that in a practical implementation, the value of R_n can be

approximated as an arbitrarily large resistance because it has relatively little impact on the cell model when studying the cell over short periods of time.

The model also includes a self-discharge resistance, R_h, for the hysteresis model. This resistance appears under the assumption that the hysteresis voltage will naturally revert back to the discharge curve after a sufficiently long period of time. This assumption is made in order to simplify the model and aid in stability analysis, but it is unclear whether this assumption is valid in reality. Like the self-discharge resistance, R_n, this resistance can be modeled as arbitrarily large without greatly affecting the performance of the model. For the sake of practicality, it is assumed that $R_h = R_n$.

CHAPTER FIVE: RESULTS

A. Validation of the Cell Model

To evaluate the accuracy of the lithium battery model, the model is implemented in Simulink. Cell current data collected from battery performance tests serves as the input to the model, and the output terminal voltage of this model is compared with the terminal voltage measured during the cell performance tests.

A block diagram of the cell model is presented in Figure 5.1. First, the cell current and estimated states are used in conjunction with interpolative look-up tables to calculate the cell parameters in this model. Next, the parameters are used to construct the four

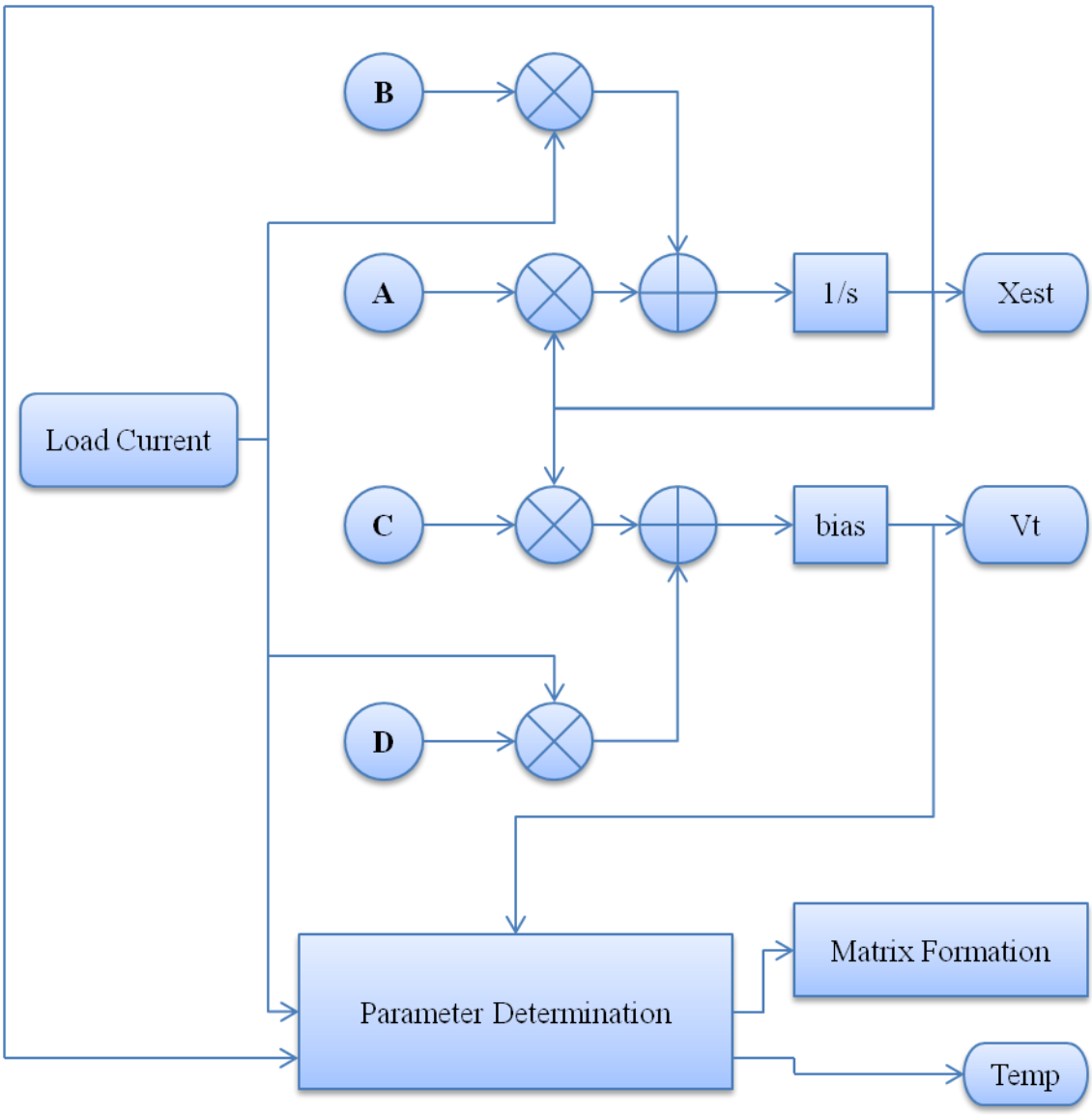

Figure 5.1: Cell model. Load current appears as the input to the model, whereas terminal voltage, state, and temperature are computed as output parameters.

matrices, $\boldsymbol{A}$, $\boldsymbol{B}$, $\boldsymbol{C}$, and $\boldsymbol{D}$, which feed a linear state-variable model, with terminal voltage acting as the model output.

The simulation is conducted on a complete pulsed discharge test at a rate of C/2. The ODE45 Dormand-Prince variable-step differential equation solver was used with a relative step tolerance 10e-3, and the simulation ran for 25e3 seconds of simulated time, taking a total of 256e3 algebraic steps. The results are presented in Figure 5.2. As a benchmark, a recent comprehensive battery model achieved an open-circuit voltage error of under $30\,mV$, and a state of charge error of less than 1.2% [16]. Similarly, an electrochemical model published in the same year achieved a maximum voltage error of under $50\,mV$ and a state of charge error of under 5% [4], whereas a maximum modeling error of $30.0\,mV$ was achieved in this test. In all three cases, the error took its maximum value during periods of transient current, but quickly settled towards a 0-mV modeling error in steady current conditions. These results indicate that the model is sufficient when compared to similar models in the literature, with the added advantage that this model lends itself well to implementation in hardware due to its simplicity and use of lookup tables.

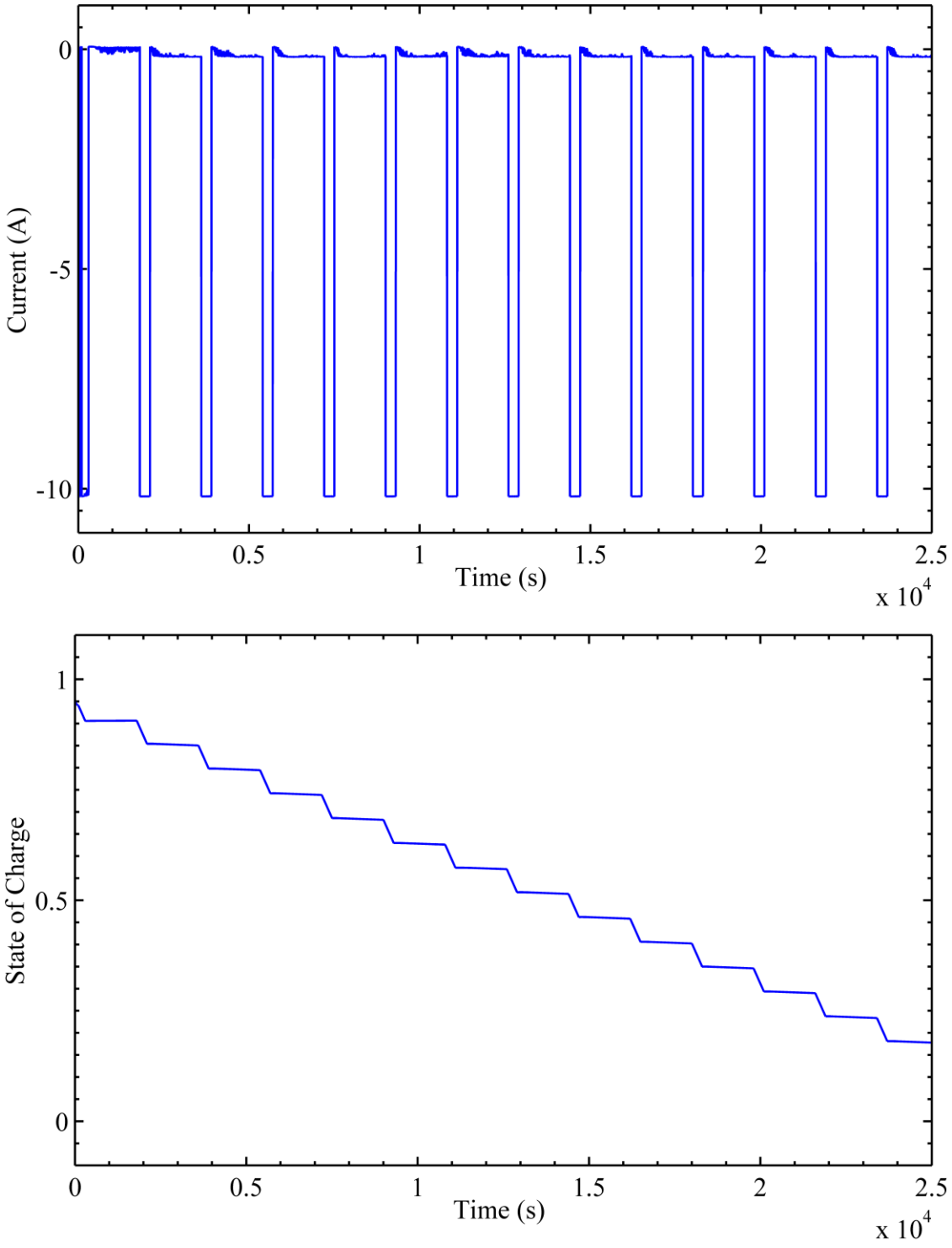

Figure 5.2: Cell model validation test results for the 10 A pulsed discharge test. The results show a maximum modeling error of under 30.0 mA.

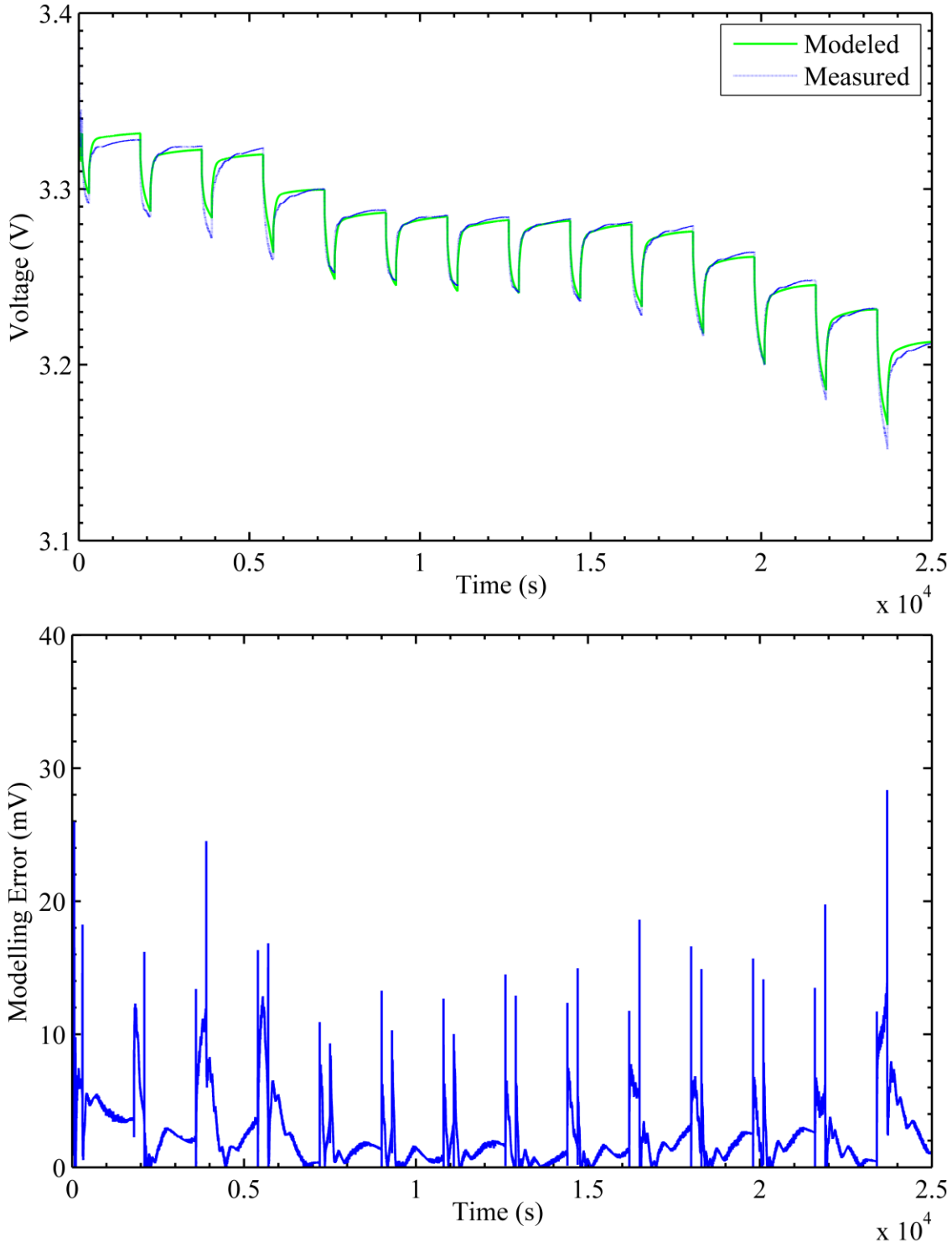

Figure 5.2 Cont'd: Cell model validation test results for the 10 A pulsed discharge test. The results show a maximum modeling error of under 30.0 mA.

B. Simulation of the Observer

In a similar manner as the cell model, the observer model has been implemented in Simulink. A block diagram of the observer appears in Figure 5.3. First, the temperature, state, and current estimate were used in conjunction with interpolative look-up tables to calculate the cell parameters used in this model. Next, the parameters were used to synthesize the matrices required for the observer. The $\boldsymbol{N}$ matrix was then pre-multiplied with the state, the $\boldsymbol{L}$ matrix was multiplied with the input, and the sum of the results fed a saturated integrator block, which insured the four states stay within their bounds. Lastly, the output equation was computed and the current and state estimates were sent to the MATLAB workspace for analysis.

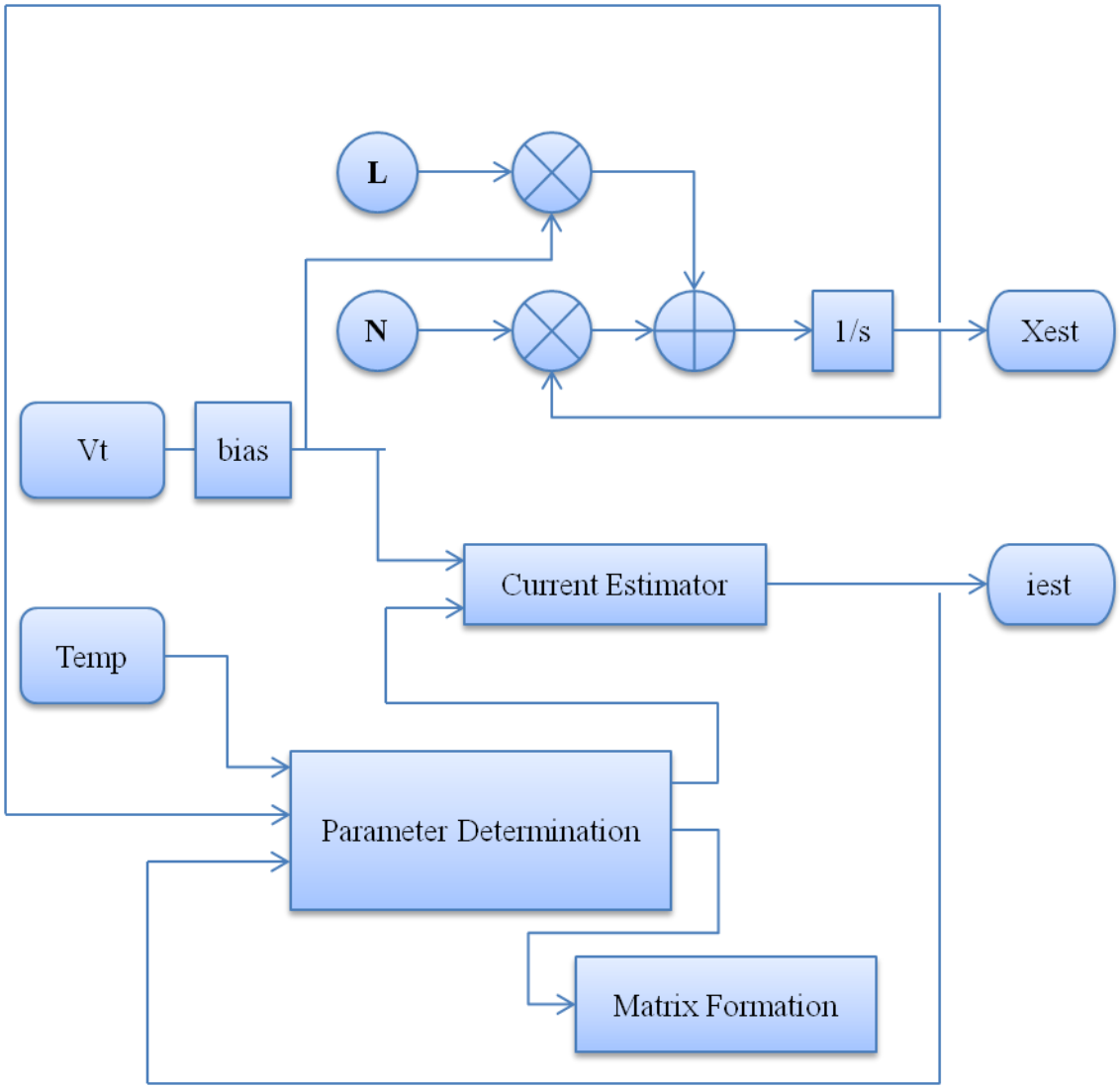

Figure 5.3: Block diagram of the unknown input observer.

The cell model was used to validate the observer. A specified current waveform was input to the cell model, which in turn produced an accurate terminal voltage to supply as an input to the observer. The current estimator output was compared to the initial current input. To provide additional insight, the estimated state variables were compared to the modeled state variables.

The Federal Urban Driving Schedule (FUDS) [48] was used as an input current waveform, and was chosen because it provides an accurate characteristic of the load current an electric vehicle battery pack might expect. This waveform is appropriate because the $LiFePO_4$ cells used in the test are marketed for use in electric vehicles, where current and power monitoring functions are essential to the diagnostics of the vehicle. FUDS is primarily a discharge test, but incorporates periods of transient charging to simulate regenerative braking in an electric vehicle. The results of the first test appear in Figure 5.4, where the initial conditions of the test were set such that the observer and the cell model began the simulation in agreement at 96% state of charge. A maximum instantaneous current estimation error of under $4\ A$ was achieved, however it is important to notice that for many applications, it will be sufficient to analyze the moving average of the current. When considering the steady-state error of current, in this case approximated by a low-pass filtered version of the current with a break frequency of $0.1\ Hz$, it was apparent that the error tended to $0\ A$.

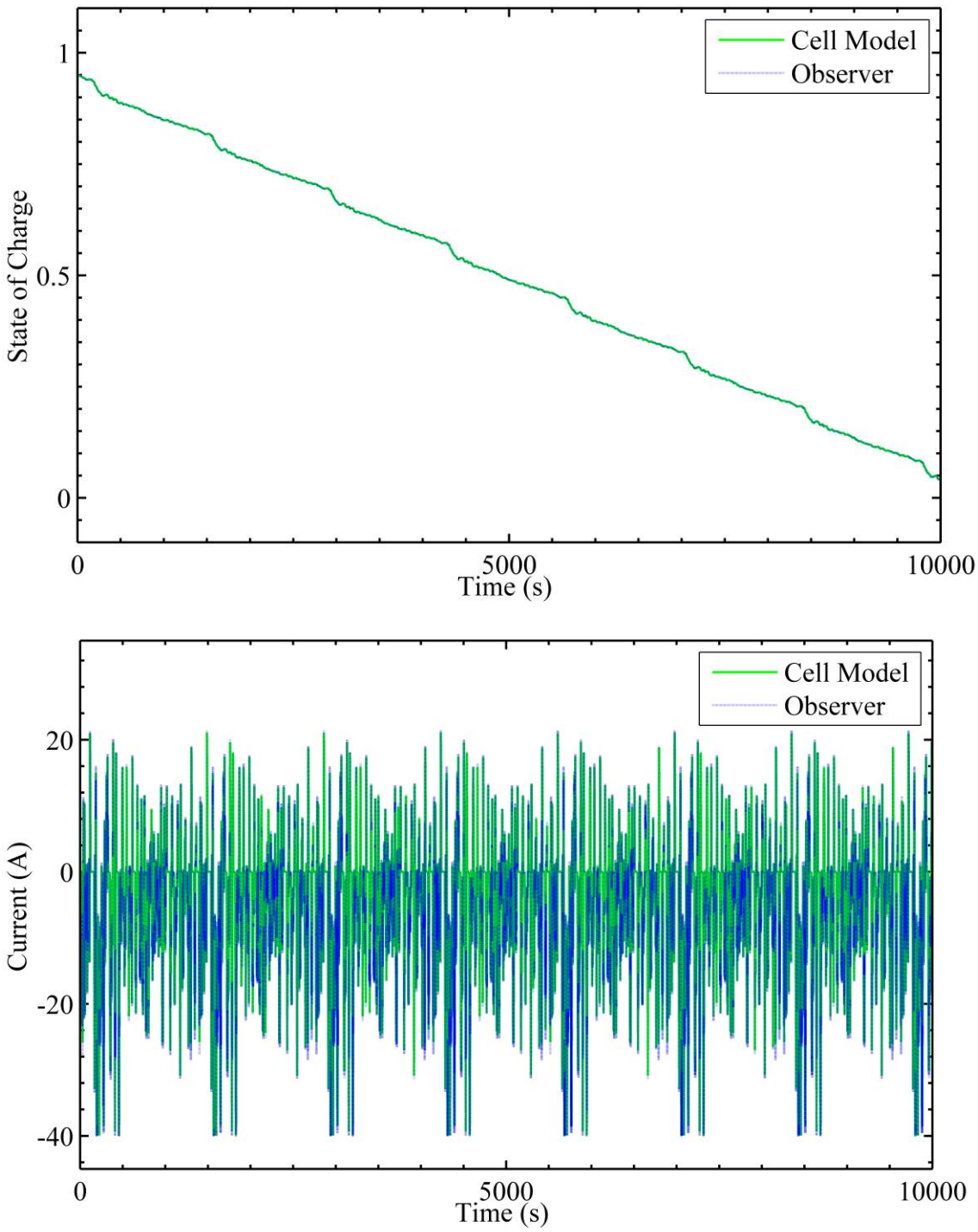

Figure 5.4: Unknown input observer model validation using FUDS current waveform. Initial conditions were set such that both the cell model and the observer model agreed at 96% state of charge. Results show that instantaneous current estimation error remained below 4 A. Additionally, a low-pass filter of 10 s was applied to the error waveform, which showed that the current error was under 2 mA when viewed in an averaged sense.

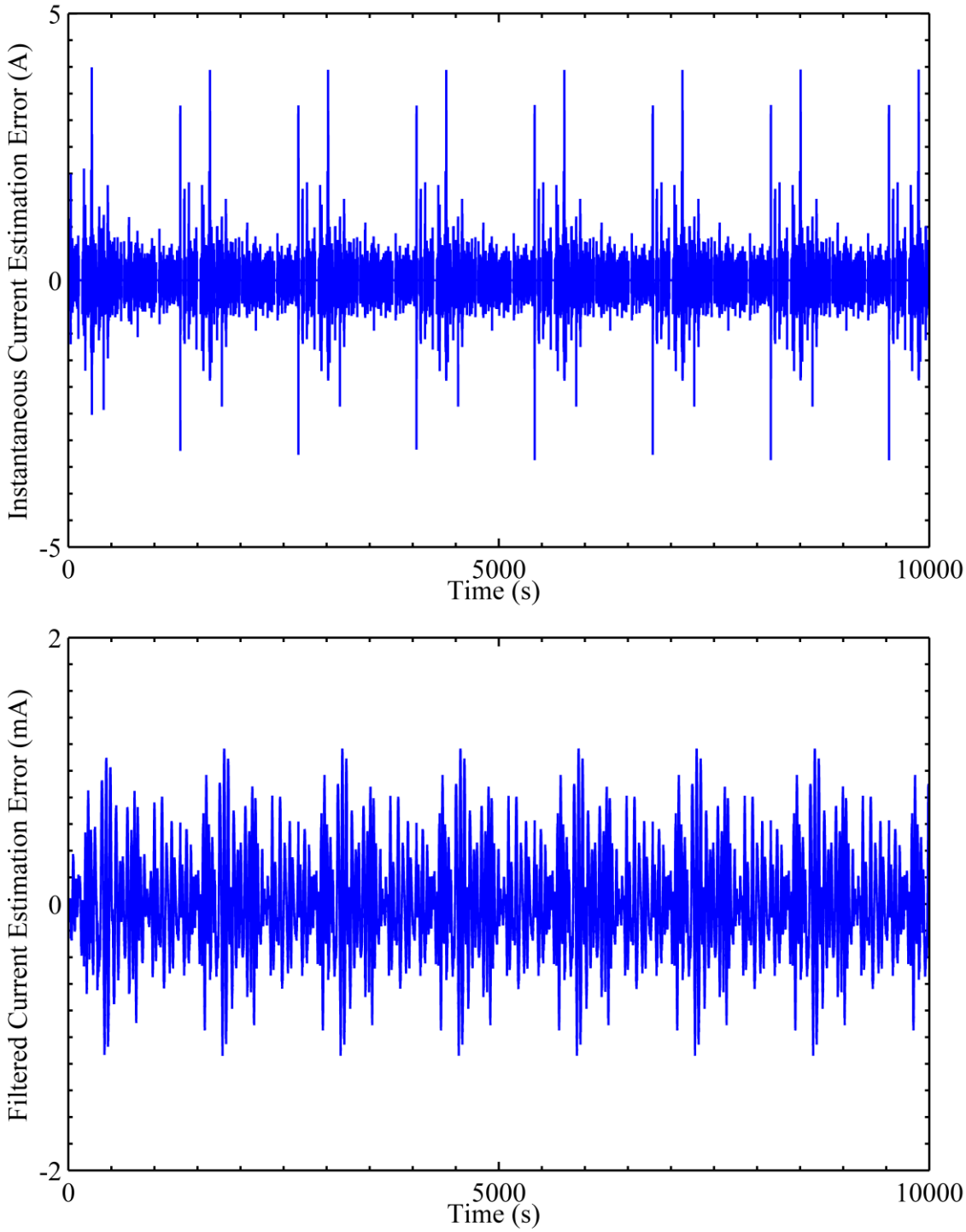

Figure 5.4 Cont'd: Unknown input observer model validation using FUDS current waveform. Initial conditions were set such that both the cell model and the observer model agreed at 96% state of charge. Results show that instantaneous current estimation error remained below 4 A. Additionally, a low-pass filter of 10 s was applied to the error waveform, which showed that the maximu current error was under 2 mA when viewed in an averaged sense.

However, one of the purposes of using an observer is to provide the ability to recover from starting with incorrect initial conditions. Thus, a second test was conducted with a 20% discrepancy in initial state of charge between the cell model and the observer. The results of this test appear in Figure 5.5. The current estimation error was greatest during periods where the state of charge estimation error was high, with filtered current estimation errors reaching as high as $9\,A$. However, the current error was significantly diminished as the state of charge estimate converged with the true value, as is expected for the observer. A 5% settling time of under 3200 s was shown for the state of charge estimate. This is indeed slower than desired in a practical application, but the settling time of the observer is uniquely determined and unable to be set for this design, which is in contrast to a standard Luenburger observer where the observer dynamics can be arbitrarily specified. Mathematically, the $\boldsymbol{N}$ and $\boldsymbol{L}$ matrices of this unknown input observer had only one solution. The unknown input observer operates with no knowledge of the input, and as a result, the degree of freedom that typically allows for pole placement has been removed.

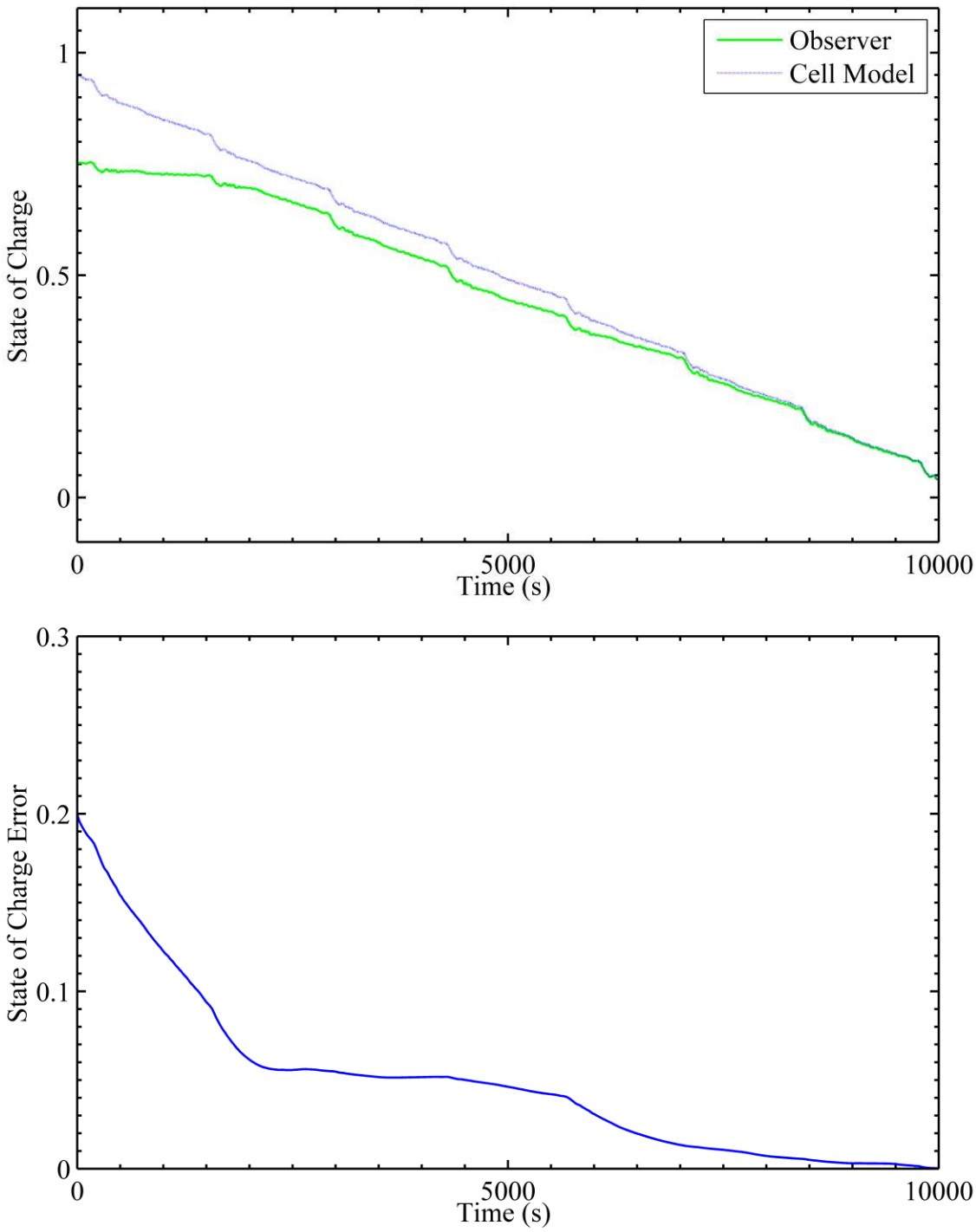

Figure 5.5: Unknown input observer model validation using FUDS current waveform with a 20% initial error in state of charge estimation. Results show a filtered current estimation error initially near 9 A but settling towards zero as the observer converged on the true states. A 5% settling time of 3200 s was observed.

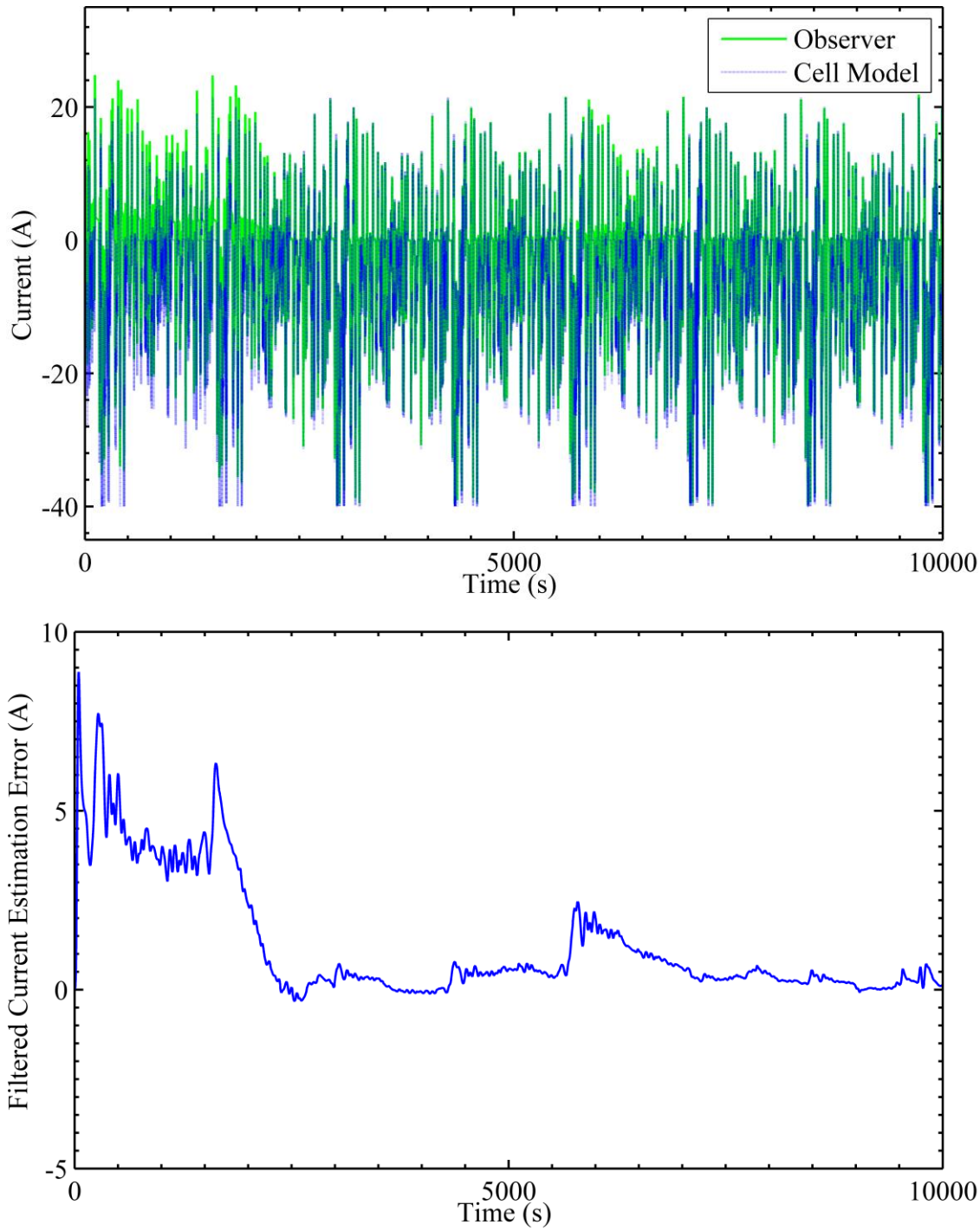

Figure 5.5 Cont'd: Unknown input observer model validation using FUDS current waveform with a 20% initial error in state of charge estimation. Results show a filtered current estimation error initially near 9 A but settling towards zero as the observer converged on the true states. A 5% settling time of 3200 s was observed.

It is important to recognize that in a practical hardware implementation of the observer, the slow settling time is not cause for concern. In a microcontroller implementation, the observer states can be periodically stored in non-volatile memory such that the BMS will always load the correct states upon initialization, provided the initial settling period has been completed. Thus, the results from Figure 5.4 are the most meaningful.

C. Experimental Validation of Hardware Implementation

The observer was implemented in a custom designed BMS containing an 8-bit, 22.1 MHz, PIC18F4580 processor. One of the objectives of this work was to develop a computationally simple method to estimate the current of a battery cell such that this method could be implemented on existing low-power, 8-bit battery management systems. As such, the processor and hardware were chosen before designing the observer, and an effort was made to develop an observer that could be realizable on the processor. The process began by transforming the observer equations into discrete time and translating the look-up tables into fixed-point look-up tables to conserve program space. There is no inherent floating-point computation unit within this processor, but floating point was desired for code-readability and precision, so the single-precision floating point library distributed with the C18 C compiler was used. The code follows the basic structure of the Simulink model. First, the state variables are initialized to estimates for their initial states. The EEPROM is used to periodically store state estimates so that on power-up, the initial conditions are set to the last known conditions of the battery cell. The voltage and temperature measurements are then taken using a 10-bit ADC. As in the Simulink model, interpolative look-up tables are used to determine the instantaneous values for the cell

parameters. These values are used to construct the observer matrices. The output is then computed and printed to a terminal over a USB connection. Lastly, the next state is computed and stored, and the process repeats for the next sample. An image of the hardware implementation and testing apparatus is provided in Figure 5.6.

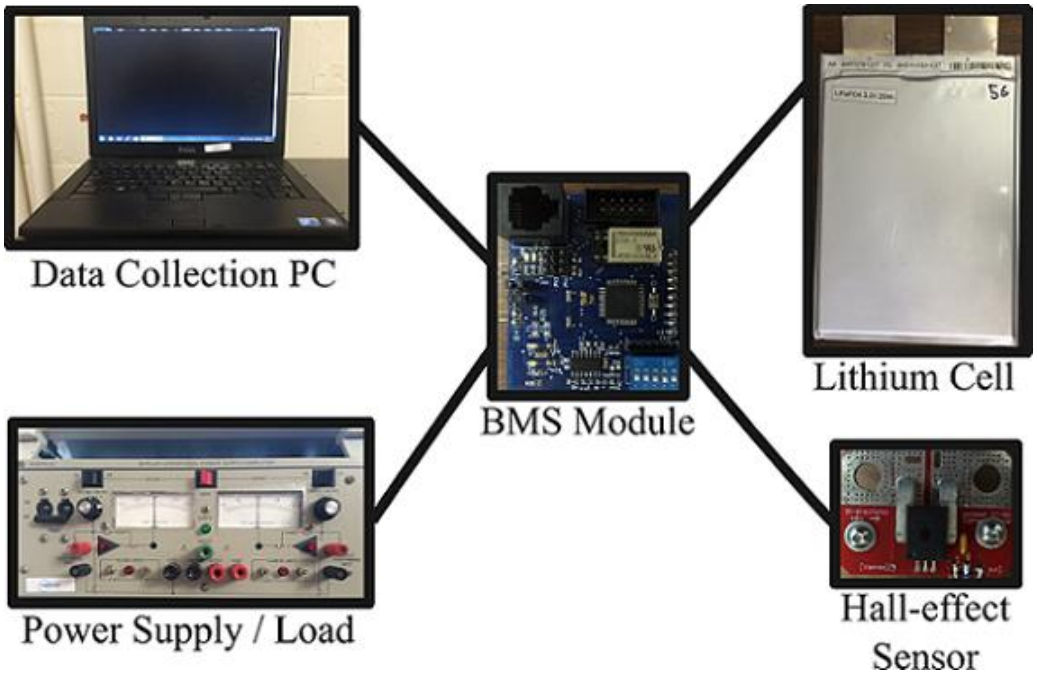

Figure 5.6: Hardware implementation of the current estimator in a custom BPS.

For this implementation, a sampling period of 0.2323 s was used, and 90% of the 16 kB in program memory was utilized, including both the observer functions and the other battery management system functions.

The testing apparatus consisted of the BMS serving as a current estimator in communication over USB to a data-logging PC. The $LiFePO_4$ cell itself was connected, through a relay controlled by the BMS, to a bidirectional power supply capable of

producing constant current sources from $-10\ A$ to $10\ A$. A Hall-effect current sensor with an error of $\pm 500\ mA$ was used to compare the results of the current estimator.

Two experiments were then conducted with the apparatus. First, a pulsed discharge cycle was carried out on the cell at a rate of $8\ A$. The results of the test are shown in Figure 5.7. From the results, it is evident the current estimator is correctly predicting that the cell is exhibiting a pulsed-discharge load pattern. The instantaneous error in current estimation peaks very high, nearly at the magnitude of the measured current; however, this is inconsequential because the peaks are caused by a slight delay between the current sensor and the current estimator. On the other hand, the filtered current error limits itself to $\pm 3\ A$, with the error tending towards zero while the cell is in a rest period.

The second experiment conducted on the cell to further characterize the dynamic estimation of current about a single state of charge. The cell current was continuously varied between $-10\ A$ and $10\ A$ over the course of a 5 minute period. The results appear in Figure 5.8, and show that in an average sense, the hardware implementation was able to estimate cell current with an accuracy of $\pm 2\ A$ whereas the instantaneous error in current estimation peaked at $\pm 5\ A$.

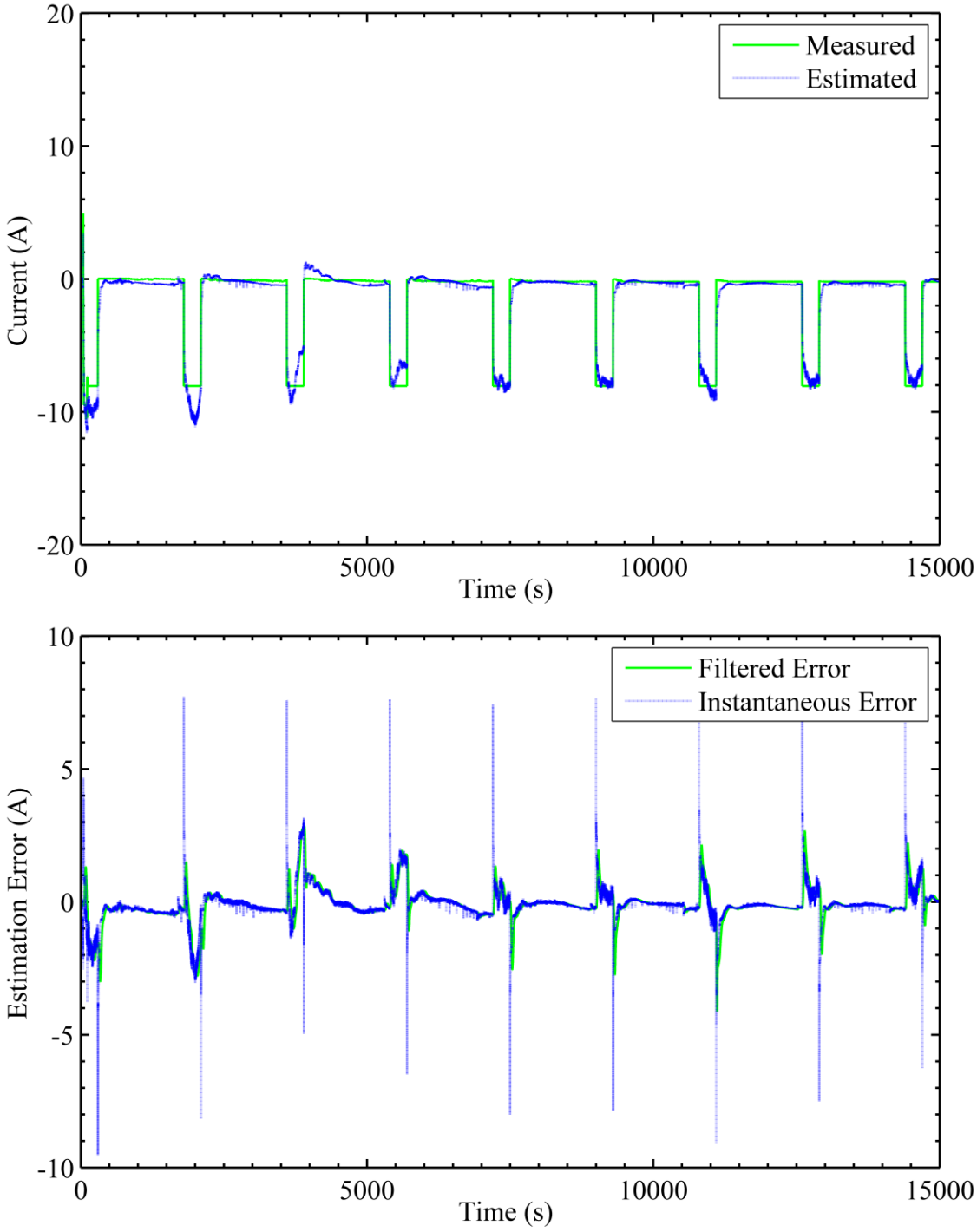

Figure 5.7: Hardware implementation results for the C/2 pulsed discharge test. The test begins with a cell at 95% state of charge and concludes with the cell discharged to 45% state of charge.

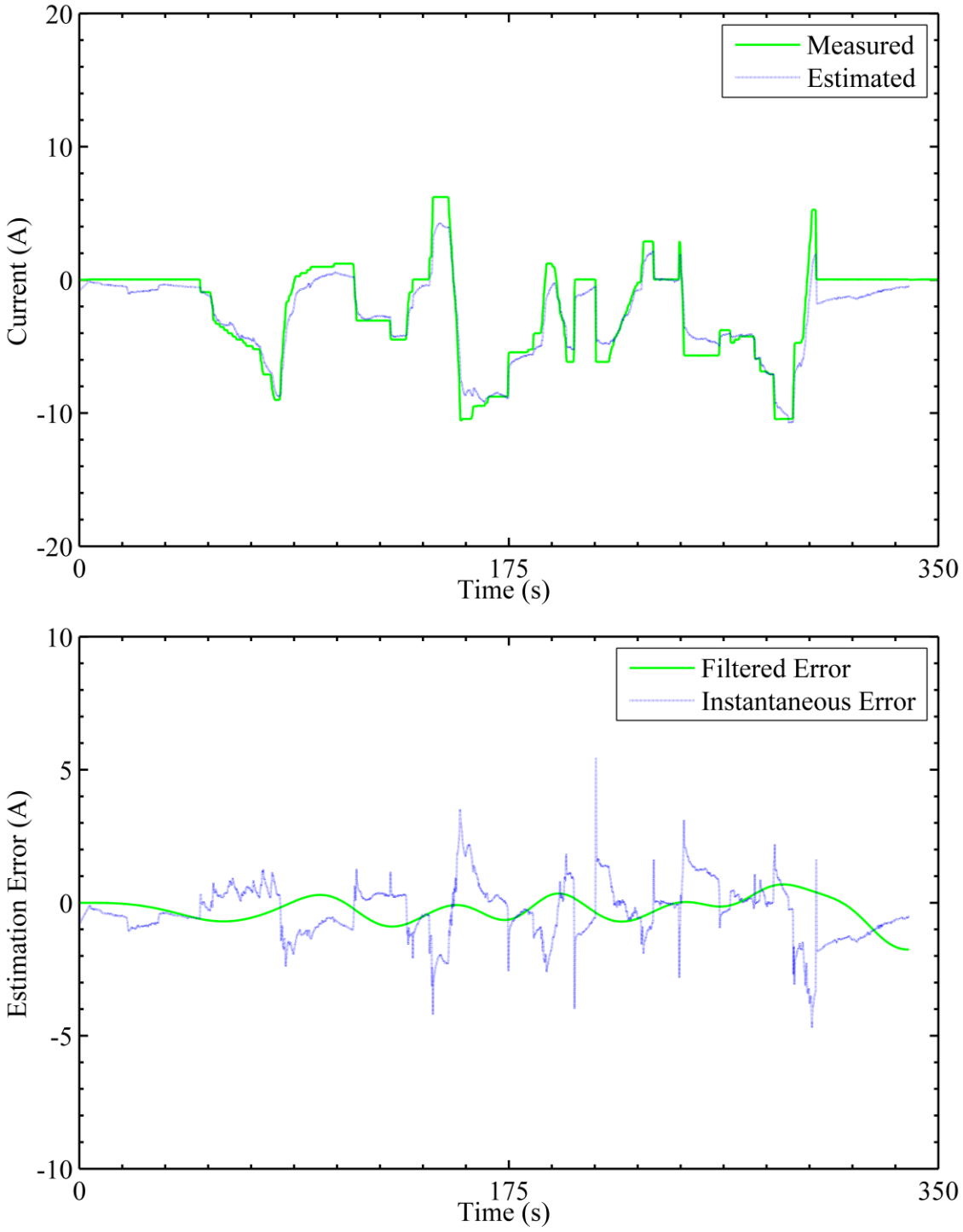

Figure 5.8: Hardware implementation results for the continuously-varying current test at 95% state of charge.

Multiple sources of error are inherently present in this problem, and they prevent the perfect reconstruction of the cell current waveform. Namely, all measured voltages used in this work had an error of $\pm 0.002\, mV$ from the sensor and the analog-to-digital conversion. Due to this fact alone, and noting that a direct feed-through term, R_0, exists between terminal voltage and load current, the load current will exhibit a minimum error of

$$\frac{\pm 0.002\, mV}{R_{0_{min}}} \approx \pm 1\, A. \tag{39}$$

This highlights the fact that extremely precise voltage measurements are required in order for this method of current estimation to be feasible; however, it also suggests that the observer current errors seen in this work are within reason when put in the context of the hardware limitations.

CHAPTER SIX: CONCLUSIONS

A practical model of a $LiFePO_4$ cell was developed which performed similarly to other models in the literature. Using this model, an unknown input observer was developed which attempted to estimate the current in the cell. The model of the current estimator was used in conjunction with the model of cell, and simulations were conducted which showed that the current estimator converged toward the true measured current. A hardware implementation was then tested, with results validating the operation of the current estimator. Although no measure of acceptability for the accuracy of the current estimation error was provided, it was shown that the current error was at least within the same order of magnitude as the Hall-effect sensor error used as a benchmark.

Future work is required to further improve the accuracy of the current estimation technique. Namely, a lithium battery pack is often comprised of multiple cells placed in series. BMSs are designed to monitor the voltage and temperature of each individual cell, thus a current estimator could be implemented for each cell comprising the battery pack. Since each estimator will produce a current estimate at a specified sampling rate, an argument can be made that the n current estimates, where n is the number of series cells in the battery pack, could combine to generate a current estimate with a greater precision and accuracy than one current estimate alone. That is, the current estimators themselves may be able to work together in dynamic consensus to produce an extremely accurate current measurement. However, there are additional problems to consider when combining cells together to form a battery pack. Often, cells are combined in series-parallel combinations such that the voltage can only be measured down to the level of a

‘module’ comprised of parallel connected cells. The observer model considered in this work only considers the dynamics of a single cell. Thus, further research in the effects of modeling parallel connected cells is required for future development. Finally, the results of this work indicate that further experimentation on the practical applications of this current estimation technique is merited. This technique could potentially be used in fault detection scenarios alongside a conventional current transducer, or as a complete replacement of a current transducer in applications where the current estimator is adequate for the required accuracy.

REFERENCES

[1] K. W. E. Cheng, B. P. Divakar, H. Wu, K. Ding, and H. F. Ho, "Battery-Management System (BMS) and SOC Development for Electrical Vehicles," *Veh. Technol. IEEE Trans. On*, vol. 60, no. 1, pp. 76–88, Jan. 2011.

[2] S. Ziegler, R. C. Woodward, H. H.-C. Iu, and L. J. Borle, "Current Sensing Techniques: A Review," *Sens. J. IEEE*, vol. 9, no. 4, pp. 354–376, Apr. 2009.

[3] O. Erdinc, B. Vural, and M. Uzunoglu, "A dynamic lithium-ion battery model considering the effects of temperature and capacity fading," in *Clean Electrical Power, 2009 International Conference on*, 2009, pp. 383–386.

[4] S. Dey, B. Ayalew, and P. Pisu, "Nonlinear Robust Observers for State-of-Charge Estimation of Lithium-Ion Cells Based on a Reduced Electrochemical Model," *Control Syst. Technol. IEEE Trans. On*, vol. 23, no. 5, pp. 1935–1942, Sep. 2015.

[5] J. Marcicki, F. Todeschini, S. Onori, and M. Canova, "Nonlinear parameter estimation for capacity fade in Lithium-ion cells based on a reduced-order electrochemical model," in *American Control Conference (ACC), 2012*, 2012, pp. 572–577.

[6] M. Rad, D. Danilov, M. Baghalha, M. Kazemeini, and P. Notten, "Thermal Modeling of Cylindrical LiFePO4 Batteries," *J. Mod. Phys.*, vol. 4, no. 7B, pp. 1–7, 2013.

[7] M. Partovibakhsh and G. Liu, "An Adaptive Unscented Kalman Filtering Approach for Online Estimation of Model Parameters and State-of-Charge of Lithium-Ion Batteries for Autonomous Mobile Robots," *Control Syst. Technol. IEEE Trans. On*, vol. 23, no. 1, pp. 357–363, Jan. 2015.

[8] C. Lin, X. Zhang, R. Xiong, and F. Zhou, "A novel approach to state of charge estimation using extended Kalman filtering for lithium-ion batteries in electric vehicles," in *Transportation Electrification Asia-Pacific (ITEC Asia-Pacific), 2014 IEEE Conference and Expo*, 2014, pp. 1–6.

[9] M. Daboussy, D. Chrenko, E.-H. Aglzim, Z. H. Che Daud, and L. Le Moyne, "Characterisation of a commercial automotive lithium ion battery using extended Kalman filter," in *Transportation Electrification Conference and Expo (ITEC), 2013 IEEE*, 2013, pp. 1–6.

[10] T. Wang, L. Pei, R. Lu, C. Zhu, and G. Wu, "Online Parameter Identification for Lithium-Ion Cell in Battery Management System," in *Vehicle Power and Propulsion Conference (VPPC), 2014 IEEE*, 2014, pp. 1–6.

[11] J. Xu, C. C. Mi, B. Cao, J. Deng, Z. Chen, and S. Li, "The State of Charge Estimation of Lithium-Ion Batteries Based on a Proportional-Integral Observer," *Veh. Technol. IEEE Trans. On*, vol. 63, no. 4, pp. 1614–1621, May 2014.

[12] H. Chaoui, N. Golbon, I. Hmouz, R. Souissi, and S. Tahar, "Lyapunov-Based Adaptive State of Charge and State of Health Estimation for Lithium-Ion Batteries," *Ind. Electron. IEEE Trans. On*, vol. 62, no. 3, pp. 1610–1618, Mar. 2015.

[13] H. Xiaosong, S. Fengchun, Z. Yuan, and P. Huei, "Online estimation of an electric vehicle Lithium-Ion battery using recursive least squares with forgetting," in *American Control Conference (ACC), 2011*, 2011, pp. 935–940.

[14] E. Leksono, I. N. Haq, M. Iqbal, F. X. N. Soelami, and I. G. N. Merthayasa, "State of charge (SoC) estimation on LiFePO4 battery module using Coulomb counting methods with modified Peukert," in *Rural Information Communication Technology and Electric-Vehicle Technology (rICT ICeV-T), 2013 Joint International Conference on*, 2013, pp. 1–4.
[15] T. Gallien, B. Schweighofer, M. Recheis, and H. Wegleiter, "State of charge determination of LiFePO4 batteries using an external applied magnetic field," in *Industrial Electronics Society, IECON 2013 - 39th Annual Conference of the IEEE*, 2013, pp. 4000–4004.
[16] M. Gholizadeh and F. R. Salmasi, "Estimation of State of Charge, Unknown Nonlinearities, and State of Health of a Lithium-Ion Battery Based on a Comprehensive Unobservable Model," *Ind. Electron. IEEE Trans. On*, vol. 61, no. 3, pp. 1335–1344, Mar. 2014.
[17] N. Lin, S. Ci, and H. Li, "An enhanced circuit-based battery model with considerations of temperature effect," in *Energy Conversion Congress and Exposition (ECCE), 2014 IEEE*, 2014, pp. 3985–3989.
[18] Low Wen Yao, J. A. Aziz, Pui Yee Kong, and N. R. N. Idris, "Modeling of lithium-ion battery using MATLAB/simulink," in *Industrial Electronics Society, IECON 2013 - 39th Annual Conference of the IEEE*, 2013, pp. 1729–1734.
[19] L. Xiwen, M. Yan, and Y. Zhenhua, "Research of SOC estimation for lithium-ion battery of electric vehicle based on AMEsim-simulink co-simulation," in *Control Conference (CCC), 2013 32nd Chinese*, 2013, pp. 7680–7685.
[20] L. Lam, P. Bauer, and E. Kelder, "A practical circuit-based model for Li-ion battery cells in electric vehicle applications," in *Telecommunications Energy Conference (INTELEC), 2011 IEEE 33rd International*, 2011, pp. 1–9.
[21] R. C. Kroeze and P. T. Krein, "Electrical battery model for use in dynamic electric vehicle simulations," in *Power Electronics Specialists Conference, 2008. PESC 2008. IEEE*, 2008, pp. 1336–1342.
[22] M. Swierczynski, D.-I. Stroe, A.-I. Stan, R. Teodorescu, and S. K. Kaer, "Investigation on the Self-discharge of the LiFePO4/C nanophosphate battery chemistry at different conditions," in *Transportation Electrification Asia-Pacific (ITEC Asia-Pacific), 2014 IEEE Conference and Expo*, 2014, pp. 1–6.
[23] D. Liu, J. Zhou, H. Liao, Y. Peng, and X. Peng, "A Health Indicator Extraction and Optimization Framework for Lithium-Ion Battery Degradation Modeling and Prognostics," *Syst. Man Cybern. Syst. IEEE Trans. On*, vol. 45, no. 6, pp. 915–928, Jun. 2015.
[24] S. Bangaru, R. Alugonda, and P. Palacharla, "Modeling and simulation of lithium-ion battery with hysteresis for industrial applications," in *Energy Efficient Technologies for Sustainability (ICEETS), 2013 International Conference on*, 2013, pp. 771–775.
[25] H. Zhang and M.-Y. Chow, "On-line PHEV battery hysteresis effect dynamics modeling," in *IECON 2010 - 36th Annual Conference on IEEE Industrial Electronics Society*, 2010, pp. 1844–1849.
[26] F. Baronti, N. Femia, R. Saletti, C. Visone, and W. Zamboni, "Hysteresis Modeling in Li-Ion Batteries," *Magn. IEEE Trans. On*, vol. 50, no. 11, pp. 1–4, Nov. 2014.

[27] F. Baronti, W. Zamboni, N. Femia, R. Roncella, and R. Saletti, “Experimental analysis of open-circuit voltage hysteresis in lithium-iron-phosphate batteries,” in *Industrial Electronics Society, IECON 2013 - 39th Annual Conference of the IEEE*, 2013, pp. 6728–6733.
[28] F. Baronti, N. Femia, R. Saletti, and W. Zamboni, “Comparing open-circuit voltage hysteresis models for lithium-iron-phosphate batteries,” in *Industrial Electronics Society, IECON 2014 - 40th Annual Conference of the IEEE*, 2014, pp. 5635–5640.
[29] L. Gagneur, C. Forgez, and A. L. D. Franco, “Lithium-ion state of charge observer with open circuit voltage hysteresis model,” in *Power Electronics and Applications (EPE), 2013 15th European Conference on*, 2013, pp. 1–7.
[30] D. Koenig and S. Mammar, “Design of proportional-integral observer for unknown input descriptor systems,” *Autom. Control IEEE Trans. On*, vol. 47, no. 12, pp. 2057–2062, Dec. 2002.
[31] M. A. Duarte-Mermoud and P. S. La Rosa, “Designing SISO observers with unknown input,” *IMA J. Math. Control Inf.*, vol. 20, no. 4, pp. 387–391, 2003.
[32] T. Raff, F. Lachner, and F. Allgower, “A Finite Time Unknown Input Observer For Linear Systems,” in *Control and Automation, 2006. MED ’06. 14th Mediterranean Conference on*, 2006, pp. 1–5.
[33] M. Hou and P. C. Müller, “Design of observers for linear systems with unknown inputs,” *Autom. Control IEEE Trans. On*, vol. 37, no. 6, pp. 871–875, Jun. 1992.
[34] F. Yang and R. W. Wilde, “Observers for linear systems with unknown inputs,” *Autom. Control IEEE Trans. On*, vol. 33, no. 7, pp. 677–681, Jul. 1988.
[35] J. Chen, R. J. Patton, and H.-Y. Zhang, “Design of unknown input observers and robust fault detection filters,” *Int. J. Control*, vol. 63, no. 1, pp. 85–105, 1996.
[36] C.-C. Tsui, “A new design approach to unknown input observers,” *Autom. Control IEEE Trans. On*, vol. 41, no. 3, pp. 464–468, Mar. 1996.
[37] M. Darouach, M. Zasadzinski, and S. J. Xu, “Full-order observers for linear systems with unknown inputs,” *Autom. Control IEEE Trans. On*, vol. 39, no. 3, pp. 606–609, Mar. 1994.
[38] S. P. Bhattacharyya, “Observer design for linear systems with unknown inputs,” *Autom. Control IEEE Trans. On*, vol. 23, no. 3, pp. 483–484, Jun. 1978.
[39] M. E. Valcher, “State observers for discrete-time linear systems with unknown inputs,” *Autom. Control IEEE Trans. On*, vol. 44, no. 2, pp. 397–401, Feb. 1999.
[40] B. Walcott and S. H. Żak, “State observation of nonlinear uncertain dynamical systems,” *Autom. Control IEEE Trans. On*, vol. 32, no. 2, pp. 166–170, Feb. 1987.
[41] M. CORLESS and J. TU, “State and Input Estimation for a Class of Uncertain Systems,” *Automatica*, vol. 34, no. 6, pp. 757 – 764, 1998.
[42] J. Moreno, “Unknown input observers for SISO nonlinear systems,” in *Decision and Control, 2000. Proceedings of the 39th IEEE Conference on*, 2000, vol. 1, pp. 790–801 vol.1.
[43] Q. P. Ha and H. Trinh, “State and input simultaneous estimation for a class of nonlinear systems,” *Automatica*, vol. 40, no. 10, pp. 1779 – 1785, 2004.
[44] A. M. Pertew, H. J. Marquezz, and Q. Zhao, “Design of unknown input observers for Lipschitz nonlinear systems,” in *American Control Conference, 2005. Proceedings of the 2005*, 2005, pp. 4198–4203 vol. 6.

[45] G. Feng, “Stability analysis of piecewise discrete-time linear systems,” *Autom. Control IEEE Trans. On*, vol. 47, no. 7, pp. 1108–1112, Jul. 2002.
[46] C.-T. Chen, *Linear System Theory and Design*, 3rd ed. New York, NY, USA: Oxford University Press, Inc., 1998.
[47] “Battery Pack Design, Validation, and Assembly Guide using A123 Systems AMP20m1HD-A Nanophosphate Cells.” A123 Systems, LLC., 2014.
[48] “Electric Vehicle Battery Test Procedures Manual.” United States Advanced Battery Consortium, Jan-1996.
[49] X. Gong, R. Xiong, and C. C. Mi, “Study of the Characteristics of Battery Packs in Electric Vehicles With Parallel-Connected Lithium-Ion Battery Cells,” *Ind. Appl. IEEE Trans. On*, vol. 51, no. 2, pp. 1872–1879, Mar. 2015.
[50] J. Zhang and S. Ci, “State of charge modeling of arbitrary cell connection,” in *Energy Conversion Congress and Exposition (ECCE), 2010 IEEE*, 2010, pp. 1635–1639.
[51] Y. Tripathy, A. McGordon, J. Marco, and M. Gama-Valdez, “State-of-Charge estimation algorithms and their implications on cells in parallel,” in *Electric Vehicle Conference (IEVC), 2014 IEEE International*, 2014, pp. 1–6.

VITA

Daniel Cambron received his B.S. in electrical and computer engineering from the University of Kentucky in 2015. Since then he has pursued his M.S. in electrical engineering, also at the University of Kentucky. While enrolled, Daniel received the Charles LeGeyt Fortescue scholarship, the Richard Merwin scholarship, and the Power and Energy Society scholarship, all from the Institute of Electrical and Electronics Engineers. He received a fellowship from the Tennessee Valley Authority, and was also awarded the Alumni Leadership award by the College of Engineering and the Robert L. Cosgriff award by the Department of Electrical and Computer Engineering. His research interests include power electronics, controls, and embedded systems.